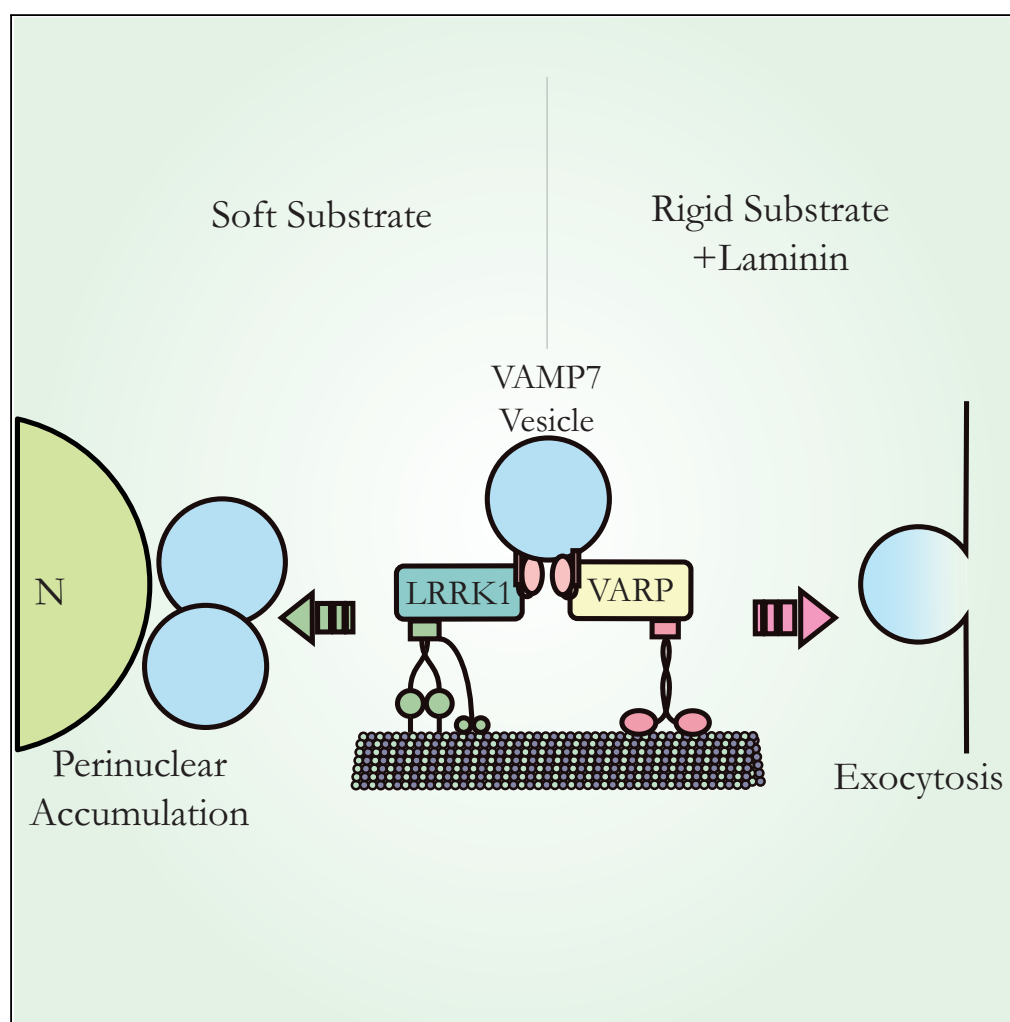**Article**

Biomechanical Control of Lysosomal Secretion Via the VAMP7 Hub: A Tug-of-War between VARP and LRRK1

Guan Wang,
Sébastien Nola,
Simone Bovio,
Philippe Bun,
Maïté Coppey-Moisan, Frank
Lafont, Thierry
Galli

thierry.galli@inserm.fr

HIGHLIGHTS

VAMP7 is important for
mechano-adaptation to
the rigidity of cellular
environment

Substrate rigidity
regulates VAMP7
exocytosis

LRRK1 and VARP compete
for VAMP7 binding

LRRK1 and VARP generate
a tug-of-war for the
transport of VAMP7

Article

Biomechanical Control of Lysosomal Secretion Via the VAMP7 Hub: A Tug-of-War between VARP and LRRK1

Guan Wang,[1,2,6] Sébastien Nola,[1,2] Simone Bovio,[3] Philippe Bun,[4] Maïté Coppey-Moisan,[5] Frank Lafont,[3] and Thierry Galli[1,2,7,*]

SUMMARY

The rigidity of the cell environment can vary tremendously between tissues and in pathological conditions. How this property may affect intracellular membrane dynamics is still largely unknown. Here, using atomic force microscopy, we show that cells deficient in the secretory lysosome v-SNARE VAMP7 are impaired in adaptation to substrate rigidity. Conversely, VAMP7-mediated secretion is stimulated by more rigid substrate and this regulation depends on the Longin domain of VAMP7. We further find that the Longin domain binds the kinase and retrograde trafficking adaptor LRRK1 and that LRRK1 negatively regulates VAMP7-mediated exocytosis. Conversely, VARP, a VAMP7- and kinesin 1-interacting protein, further controls the availability for secretion of peripheral VAMP7 vesicles and response of cells to mechanical constraints. LRRK1 and VARP interact with VAMP7 in a competitive manner. We propose a mechanism whereby biomechanical constraints regulate VAMP7-dependent lysosomal secretion via LRRK1 and VARP tug-of-war control of the peripheral pool of secretory lysosomes.

INTRODUCTION

From the softest tissue like the brain (<1 kPa) to the hardest ones like bones (~100 kPa), the stiffness of cell environment can greatly vary in the body of mammals. Matrix elasticity was shown to affect the differentiation of stem cells (Engler et al., 2006), cell spreading and morphology, and the capacity to migrate (Tzvetkova-Chevolleau et al., 2008). Cells adhere to the substrate and sense the rigidity of the substrate via integrin-mediated focal adhesions (Chen et al., 2015; Sun et al., 2016). Cell adhesion is able to regulate the cytoskeleton and membrane tension (Sens and Plastino, 2015). Previous work showed that exocytosis and endocytosis are regulated by cell spreading and osmotic pressure (Gauthier et al., 2011) and membrane tension regulates secretory vesicle docking through a mechanism involving Munc18-a (Papadopulos et al., 2015). How substrate rigidity sensing may regulate exocytosis, which in turn regulates membrane tension, is still largely unknown. Secretory mechanisms involve SNAREs, the master actors of intracellular membrane fusion (Südhof and Rothman, 2009). Exocytosis involves the formation of a SNARE complex comprising a vesicular SNARE (v-SNARE) on the vesicle side. Two main v-SNAREs were shown to mediate distinct exocytic mechanisms: clostridial neurotoxin-sensitive VAMP2 (and the closely related VAMP1 and VAMP3) mediates synaptic vesicle and early endosomal exocytosis, whereas clostridial neurotoxin-insensitive VAMP7 mediates Golgi-derived, late endosomal and lysosomal secretory pathways (Proux-Gillardeaux et al., 2005a), which are best defined by the presence of the tetraspanin CD63 (Chiaruttini et al., 2016; Coco et al., 1999). In the recent years, lysosomal exocytosis has appeared as a very general mechanism that can be found in virtually any cell type (Ghosh et al., 2016; Jaiswal et al., 2002; Li et al., 2008; Verderio et al., 2012). Interestingly enough, VAMP2 and VAMP3 were shown to mediate integrin recycling (Hasan and Hu, 2010; Proux-Gillardeaux et al., 2005b; Skalski and Coppolino, 2005; Tayeb et al., 2005), and VAMP7, to play an essential role in cell migration and invasion (Proux-Gillardeaux et al., 2007; Steffen et al., 2008; Williams and Coppolino, 2011). VAMP7 also contributes to the regulation of membrane composition of sphingolipids and glycosylphosphatidy-linositol (GPI)-anchored protein (Molino et al., 2015), which in turn may modulate integrin dynamics and adhesion (Eich et al., 2016; van Zanten et al., 2009). VAMP7 mediates the release of ATP (Fader et al., 2012; Verderio et al., 2012) and interleukin-12 (Chiaruttini et al., 2016) and is required for the transport of cold-sensing channel TRPM8- and lysosomal-associated membrane protein 1-containing vesicles in sensory neurons (Ghosh et al., 2016). In neurons, VAMP2 exocytosis was shown to be regulated by an

[1]Membrane Traffic in Health & Disease, Institut Jacques Monod, CNRS UMR7592, INSERM U950, Sorbonne Paris-Cité, Université Paris Diderot, Paris 75205, France

[2]Membrane Traffic in Healthy & Diseased Brain, Center of Psychiatry and Neurosciences, INSERM U894, Sorbonne Paris-Cité, Université Paris Descartes, 102-108 rue de la Santé, Paris 75014, France

[3]Cellular Microbiology and Physics of Infection Group, Center for Infection and Immunity of Lille, CNRS UMR 8204, INSERM U1019, Institut Pasteur de Lille, Centre Hospitalier Régional de Lille, Université de Lille, Lille, France

[4]NeurImag Tech Core Facility, Center of Psychiatry and Neurosciences, INSERM U894, Sorbonne Paris-Cité, Université Paris Descartes, Paris 75014, France

[5]Mechanotransduction: from Cell Surface to Nucleus, Institut Jacques Monod, CNRS UMR7592, Sorbonne Paris-Cité, Université Paris-Diderot, Paris, France

[6]Present address: Max-Planck-Institut für Biochemie, Martinsried, Germany

[7]Lead Contact

*Correspondence: thierry.galli@inserm.fr

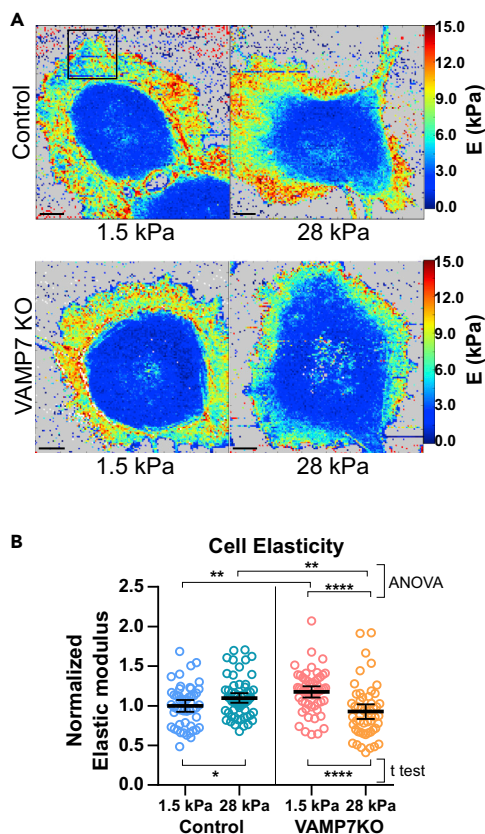https://doi.org/10.1016/j.isci.2018.05.016

Figure 1. VAMP7 Is Required for Fibroblast Mechano-Adaptation

(A) Elasticity heatmaps of cells plated on laminin-coated PDMS gels of 1.5 or 28 kPa. Measurements were systematically made in a 20-µm-wide rectangular area whose typical placement is indicated by the black box. Scale bar, 10 µm.

(B) Quantification of cell elasticity (elastic modulus E). Graph shows scatterplot with mean ± 95% confidence interval (CI). Each point represents the median E value of a cell from four independent experiments. n = 51, 62, 57, and 53 cells, respectively. *$p < 0.05$, **$p < 0.01$, and ****$p < 0.0001$; ANOVA with Tukey's post hoc or Welsh's t test was used as indicated.

integrin-independent mechanism and VAMP7 exocytosis by an integrin-, FAK-, and Src-dependent mechanism (Gupton and Gertler, 2010).

Here we used atomic force microscopy, micropatterned surfaces, pHluorin live imaging of lysosomal exocytosis (Balaji and Ryan, 2007), and substrate of controlled rigidity and composition to explore the role of lysosomal exocytosis in cell response to biomechanical constraints. Our results suggest that VAMP7-dependent lysosomal secretion responds to rigidity via control by its partners LRRK1 and VARP of the peripheral pool of secretory lysosomes.

RESULTS

VAMP7 Is Required for Fibroblast Mechano-Adaptation

Cells have the ability to adapt their internal stiffness to substrate rigidity (Solon et al., 2007). We cultured COS7 cell on soft gels with a rigidity of 1.5 and 28 kPa, mimicking brain and cartilage rigidity, respectively, and measured the cell elasticity of control and VAMP7 knockout (KO) cells by atomic force microscopy (Figure 1A). Wild-type (WT) COS7 cells had a slightly higher elasticity when plated on 28-kPa than on 1.5-kPa substrate (Figure 1B). Surprisingly, VAMP7 CRISPR/Cas9 KO cells (Figure S1) had a higher elasticity in the 1.5-kPa condition than control cells and reacted differently to the change in substrate rigidity, with a lower elasticity on a more rigid substrate. The observed difference between 1.2 and 0.9 kPa, a one-third-fold change, appeared in the range of the one observed for vimentin KO (Messica et al., 2017), suggesting a strong impact of VAMP7 KO on cell elasticity. We did not observe any visible change in cytoskeletal

organization (Figure S2A) or cell spreading area (Figure S2B) between WT and VAMP7 KO COS7 cells in our conditions, data possibly explained by the fact that COS7 cells are devoid of myosin IIa and show some contractility defects (Even-Ram et al., 2007).

To understand the potential importance of VAMP7 in cell mechanics and response to mechanical constraints, we first localized VAMP7 in COS7 cells grown on micropatterned glass coverslips coated with laminin. We used cells grown on O pattern, a pattern with homogeneous mechanical constraint as control, and Y pattern, a condition wherein cells are under peripheral traction forces (Albert and Schwarz, 2014). We found that VAMP7 was particularly enriched in actin-rich cell tips (Figures 2A and 2B), where contractile forces are generated, in cells grown on a Y pattern.

VAMP7 localizes into different post-Golgi compartments, mostly endosomal compartments, and CD63, a tetraspanin of secretory lysosomes, is the best marker colocalizing with VAMP7 described so far (Chiaruttini et al., 2016; Coco et al., 1999). Thus we analyzed the colocalization of endogenous VAMP7 and CD63 on laminin-coated glass coverslips (Figure S3A) and fluorescent protein-tagged VAMP7 and CD63 on rigidity-defined polydimethylsiloxane (PDMS) surface (Figures S3B and S3C). As expected, VAMP7 showed high level of colocalization with CD63 in all conditions. We further characterized the subcellular localization of exogenously expressed VAMP7 with APP, a protein known to traffic through late endosomes/lysosomes (Tam et al., 2014); VAMP7's partner, the adaptor AP3 (Kent et al., 2012; Martinez-Arca et al., 2003); and the endosomal markers Rab5 and Rab7 (Figure S4). Tagged VAMP7 showed similar degree of colocalization with the tested endosomal markers on both soft and rigid substrates. Thus, the subcellular targeting of VAMP7 to late endosomes and lysosomes was not significantly influenced by substrate stiffness. The level of expression of VAMP7 further appeared to have an effect on the peripheral positioning of CD63 in constrained cells. Indeed, whereas KO of VAMP7 did not significantly affect CD63 subcellular localization compared with control cells on Y micropatterns, re-expression of the protein in KO cells modified the distribution of CD63 with an enrichment in cell necks (Figures 2C and 2D) without changing its total expression level (Figure S5A) or cytoskeleton organization (Figure S5B). Altogether, these experiments show that VAMP7 participates in cell response to biomechanical constraints likely via a role in CD63+ secretory lysosome positioning.

VAMP7-Mediated Exocytosis Is Regulated by Mechanosensing

Previous studies suggested that the peripheral positioning of lysosomes is important for their secretion (Encarnação et al., 2016; Guardia et al., 2016; Hämälistö and Jäättelä, 2016; Pu et al., 2016). As lysosome position is a pre-requisite for VAMP7-mediated lysosome fusion at the plasma membrane, we wondered if mechanical cues such as substrate rigidity could directly regulate lysosomal exocytosis. We measured the individual VAMP7 and VAMP2 exocytic events using pHluorin-tagged molecules (Figure 3A, Videos S1 and S2) expressed in COS7 cells grown on surfaces of controlled stiffness generated using PDMS gels of 1.5 and 28 kPa. Here the pHluorin was attached to the luminal terminal of VAMPs as mentioned previously (Burgo et al., 2012). The fluorescence signal from pHluorin is quenched in acidic medium, as inside secretory lysosomes. After the exocytic membrane structure has undergone fusion with the plasma membrane, pHluorin appears in neutral pH extracellular medium and the fluorescence signal suddenly appears as a flash of light. Thus, the pHluorin signals are the direct consequence of SNARE complex formation and membrane fusion corresponding to secretory events. We found that the frequency of exocytosis of VAMP7 had an up to ~1.5-fold increase on 28 kPa in the presence of laminin compared with on 1.5 kPa in the absence of laminin, whereas VAMP2 exocytosis was insensitive to both substrate stiffness and chemistry (Figures 3B and 3C). This finding was confirmed using polyacrylamide gels coated with polylysine or laminin with increased rigidity, as the frequency of VAMP7 exocytosis doubled from 1.5 to 28 kPa, with already a noticeable intermediate increase at 11 kPa (Figures 3D and 3E). Previous studies have reported an ~2-fold change in exocytosis under the effect of laminin versus polylysine on glass coverslip, or under pharmaceutical disruption of cytoskeleton and integrin signaling (Gupton and Gertler, 2010). Therefore, the doubling in exocytic frequency that we observed appears to be a strong and significant effect. COS7 cells endogenously express laminin receptors integrin $\alpha3$, $\alpha6$, and $\beta1$ (Niessen et al., 1997). Integrin-dependent adhesion transduces intracellular signals, which affects actomyosin contraction (Parsons et al., 2010). Here we found that blebbistatin affected VAMP7-dependent exocytosis in a dose-dependent manner (Figure S6), further suggesting biomechanical control of VAMP7 exocytosis, likely downstream of integrin-dependent adhesion, as previously found in neurons (Gupton and Gertler, 2010).
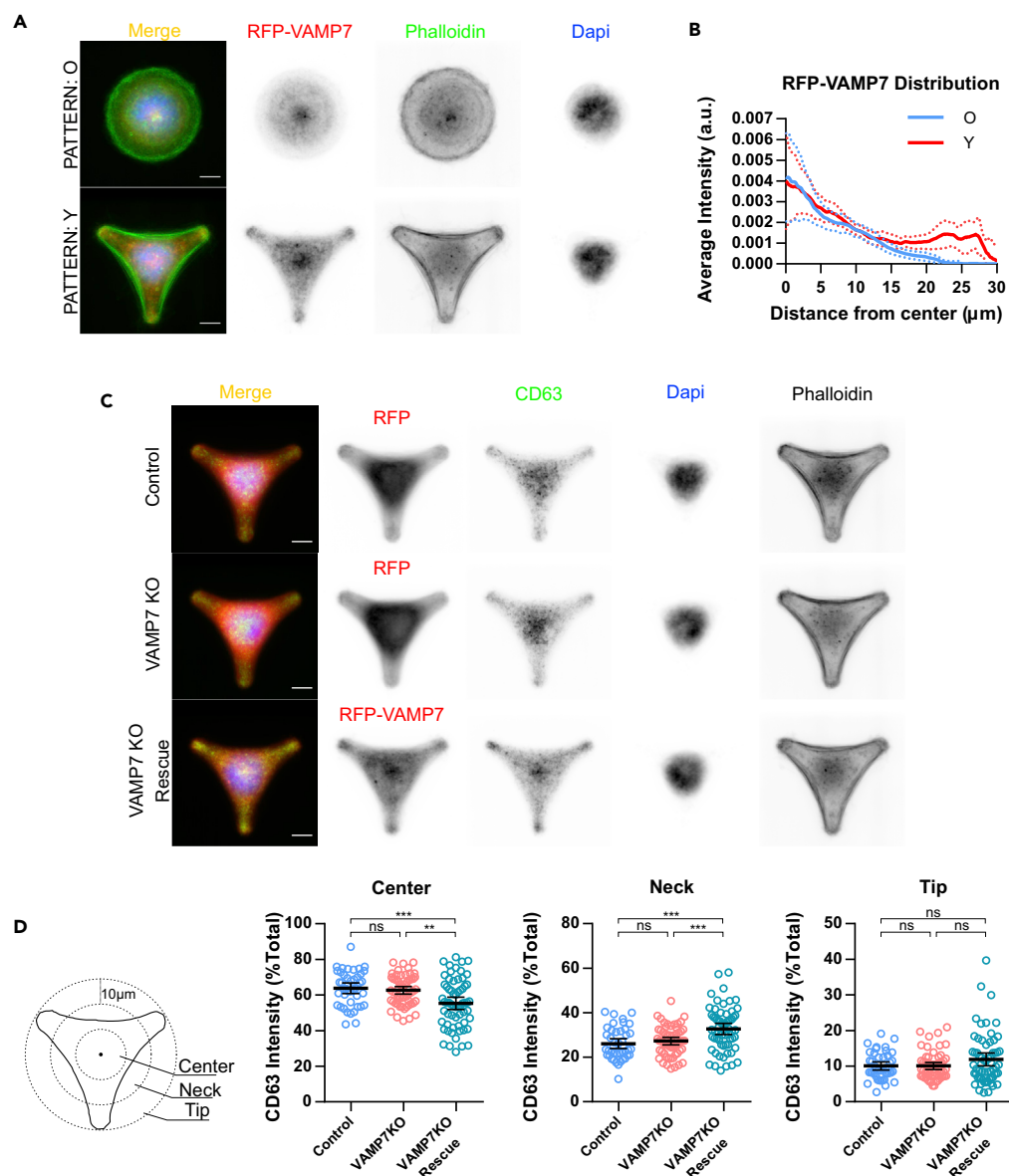
Figure 2. VAMP7 Enriches in Tips on Y-Shaped Micropattern

(A) Projection of confocal microscopy optical sections of COS7 cells plated on laminin-coated micropatterns. n: O = 27, Y = 27 cells. Scale bar, 10 μm.

(B) Quantification of RFP-VAMP7 intensity from cell center to cell periphery. Graph shows mean ± 95% confidence interval (CI) (dashed lines).

(C) Projection of confocal microscopy optical sections of control, VAMP7 KO, and VAMP7 KO re-expressing GFP-VAMP7 cells plated on Y micropatterns. n = 43, 59, and 63 cells respectively. Scale bar, 10 μm.

(D) Quantification of CD63 immunofluorescence in cell center area (<10 μm from the geometry center), neck area (between 10 and 20 μm), and tip area (>20 μm). Graph shows scatterplot with mean ± 95% CI. Each point represents the value obtained from cells from two independent experiments. **p < 0.01 and ***p < 0.001; ANOVA with Tukey's post hoc. ns, not significant.

Longin-Dependent Regulation of VAMP7 Exocytosis by Mechanosensing

Then, we asked whether the regulation of VAMP7 exocytosis could be due to the presence of the Longin domain (LD), the main regulator of VAMP7 (Daste et al., 2015). Indeed, we found that a mutant of VAMP7 lacking the LD (Δ[1-125]-VAMP7) showed increased exocytosis as previously described (Burgo et al., 2013), but its exocytic frequency was not affected by the substrate stiffness and chemistry and was already
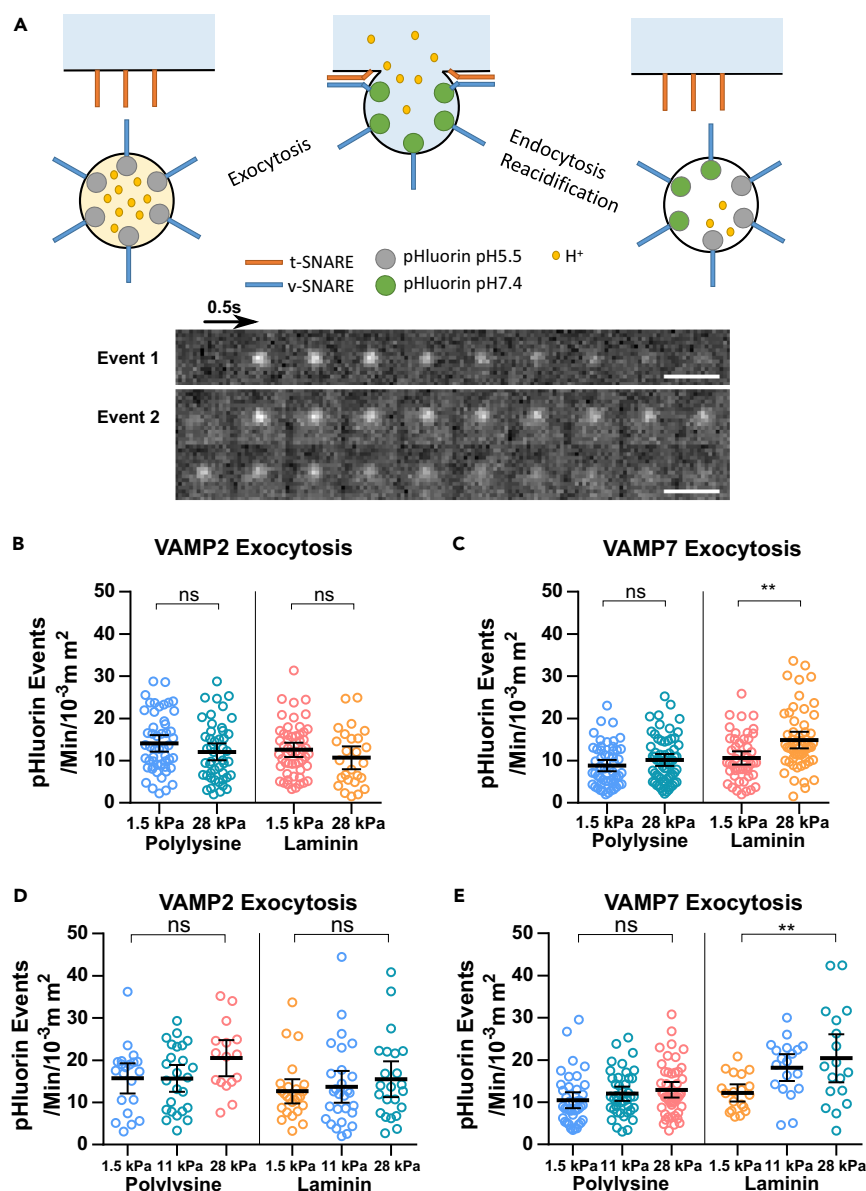
Figure 3. VAMP7-Mediated Exocytosis Is Regulated by Mechanosensing

(A) Principle of exocytic membrane fusion imaging with pHluorin. Upper panel: pHluorin was attached to the luminal terminal of VAMP2 and VAMP7. The fluorescence signal from pHluorin is quenched in acidic medium, as inside secretory vesicles. After the vesicles undergo fusion with the plasma membrane, pHluorin is exposed to the neutral pH of extracellular medium and the fluorescence signal suddenly appears as a flash of light. Lower panel: representative snapshots of two typical individual exocytic events of short (1) and long (2) life time as shown by persistence of the fluorescence signal. Scale bar: 1 μm, 0.5 s per image.

(B and C) Quantification of exocytic events in COS7 cells expressing pHluorin-tagged VAMP2 or VAMP7. Cells were plated on polylysine- or laminin-coated PDMS gel of 1.5 or 28 kPa for 18–24 hr. Graph shows scatterplot with mean ± 95% confidence interval (CI). Each point represents the exocytic rate of cells from two or more independent experiments. (B) n = 51, 48, 54, and 26; (C) n = 54, 62, 49, and 55 cells, respectively. **p < 0.01, Welsh's t test. ns, not significant.

(D and E) Quantification of exocytic events in COS7 cells expressing pHluorin-tagged VAMP2 and VAMP7. Cells were plated on polylysine- or laminin-coated polyacrylamide gel of 1.5, 11, or 28 kPa for 18–24 hr. Graph shows scatterplot with mean ± 95% CI. Each point represents the exocytic rate of cells from two or more independent experiments. VAMP2: n = 21, 25, 16, 25, 28, and 23; VAMP7, n = 40, 41, 47, 19, 19, and 18 cells, respectively. **p < 0.01, Welsh's t test.
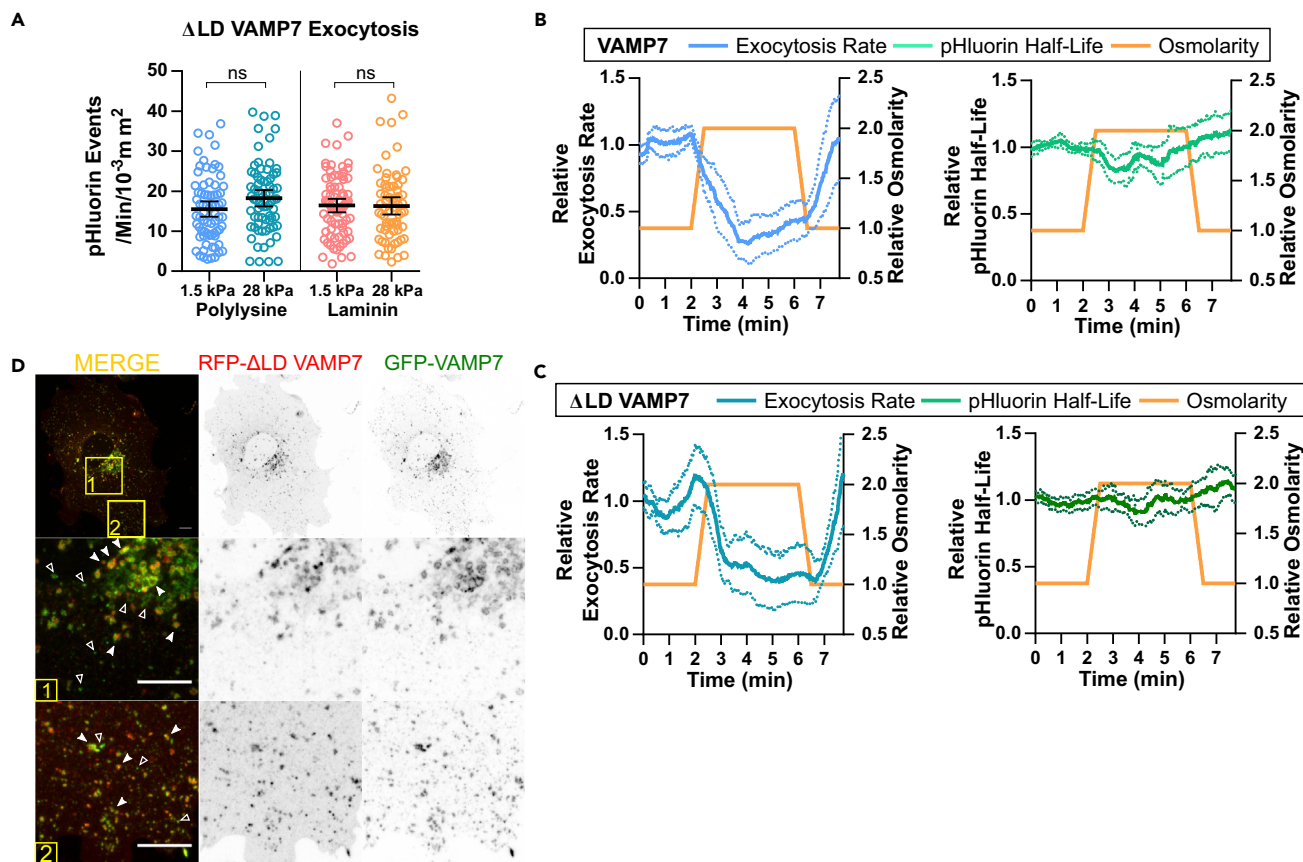
Figure 4. Mechanoregulation of VAMP7 Exocytosis by Substrate Rigidity Specifically Requires Longin Domain

(A) Quantification of exocytic events in COS7 cells expressing pHluorin-tagged ΔLD(Δ[1–125]) VAMP7. Cells were plated on polylysine- or laminin-coated PDMS gel of 1.5 or 28 kPa for 18–24 hr. Graph shows scatterplot with mean ± 95% confidence interval (CI). Each point represents the exocytic rate of cells from two or more independent experiments. n = 72, 72, 80, and 67 cells, respectively. Welsh's t test.

(B and C) Quantification of exocytic rate and pHluorin signals' half-life in COS7 cells expressing pHluorin-tagged VAMP7 or ΔLD-VAMP7. Cells were plated on laminin-coated 28-kPa PDMS gels for 18–24hr. Hyper-osmotic shocks were performed by perfusing the 2x osmolality buffer and then washed out by 1x buffer. At each time point, the exocytic rate in the following minute was calculated. Graph shows mean ± 95% CI (dashed lines). B, n = 13; C, n = 11, pooled from two or more independent experiments.

(D) Representative COS7 cell co-expressing RFP-tagged ΔLD(Δ[1–120]) VAMP7 and GFP-tagged full-length VAMP7. Filled arrowheads show the colocalization. Empty arrowheads indicate structures containing only GFP-VAMP7. Scale bar, 10 μm.

maximal on soft substrate (Figure 4A, to be compared with WT VAMP7, Figure 3C). We further analyzed the half-life of pHluorin signals, which represents the kinetics of fusion pore opening and spreading followed by endocytosis and re-acidification (Figure S7A). VAMP2, VAMP7, and ΔLD-VAMP7 showed no significant difference in signal persistence depending on stiffness and chemistry. Altogether, these data suggest that VAMP7 exocytosis is modulated by substrate stiffness and composition in an LD-dependent manner. This mode of regulation did not appear to affect the mode of fusion (i.e., transient fusion versus full fusion [Yudowski et al., 2006]) and thus most likely affects the pool size and/or release probability of secretory VAMP7+ vesicles. VAMP7 and VAMP2 interact with the same plasma membrane target-SNAREs (t-SNAREs) to mediate exocytosis in non-neuronal cells, i.e., syntaxin 4 and SNAP23 (Martinez-Arca et al., 2001; Rao et al., 2004; Sander et al., 2008). Our results showing that VAMP2 exocytosis was insensitive to rigidity thus further suggested that t-SNAREs are likely not regulated by substrate rigidity. The previous results suggested that substrate stiffness could have a specific role in VAMP7 regulation. To more directly test the hypothesis of the role of membrane tension in VAMP7 exocytosis, we used hyper-osmotic changes and pHluorin imaging as mentioned previously. We found that high hyper-osmotic pressure (2x osmolality) could instantaneously and reversibly reduce the exocytosis frequency of VAMP7 independently of its LD, suggesting different mechanisms of action of membrane tension modulated by osmotic changes and substrate stiffness (Figures 4B and 4C, Video S3). We also found that the half-life of pHluorin signals was

moderately decreased following hyperosmotic shocks and then spontaneously restored to a normal level. ΔLD-VAMP7 colocalized with full-length VAMP7 in the cell periphery but was absent in some perinuclear endosomes (Figure 4D), likely corresponding to late endosomes and lysosomes where VAMP7 is targeted in an LD/AP3-dependent manner (Kent et al., 2012; Martinez-Arca et al., 2003). Therefore, these experiments suggest that substrate rigidity specifically affects lysosomal secretion (VAMP7) and not early endosomal recycling (VAMP2, ΔLD-VAMP7).

Altogether, pHluorin imaging experiments led us to propose that membrane tension (such as modulated by osmotic shocks) is a master regulator of exocytosis independent of vesicle origin (both endosomal and lysosomal). On the contrary, the regulation of VAMP7 by substrate stiffness appeared to not depend on a pure biomechanical effect via plasma membrane tension but rather required proper sensing of the environment rigidity, such as in the presence of laminin.

Role of VAMP7 Hub in Mechanosensing

VAMP7 interactome includes two proteins connected to molecular motors. LRRK1 interacts with VAMP7 through its ankyrin repeat and leucine-rich repeat domain and also interacts with dynein (Kedashiro et al., 2015a; Toyofuku et al., 2015). The Rab21 guanine nucleotide exchange factor VARP interacts with VAMP7 through a small domain in its ankyrin repeat domains and also interacts with kinesin 1 (Burgo et al., 2009, 2012; Schäfer et al., 2012). Interestingly, sequence analysis showed that the ankyrin repeat of VARP, which interacts with VAMP7, includes a 10-amino acid (aa) sequence fully conserved in LRRK1 (Figure 5A). This led us to wonder whether or not LRRK1 and VARP may participate in the regulation of VAMP7 by substrate stiffness via its LD, in a potentially competitive manner. First, to determine whether the interaction between VAMP7 and LRRK1 was through the LD, we carried out in vitro binding assay with GST-tagged cytosolic domain (Cyto) and LD of VAMP7 protein. We found that LRRK1 had an ~10-fold stronger interaction with LD than with the cytosolic portion of the protein (Figures S8A and S8B). Next, we immunoprecipitated GFP-tagged LRRK1 or GFP-tagged VARP and assayed for coprecipitation of red fluorescent protein (RFP)-tagged full length and various deleted forms of VAMP7 (Figure 5B) from transfected COS7 cells. We found that LRRK1 interacted with full length, LD, and SNARE domain, whereas the interaction of VARP was preferentially with full length and SNARE domain, with weak binding to the LD alone (Figures 5C and 5D, Tables S1 and S2). The spacer between LD and SNARE domain alone did not bind to either LRRK1 or VARP, but appeared to increase the binding of SNARE domain to both LRRK1 and VARP. This likely indicates that the spacer could help the folding of the SNARE domain required for interaction with both LRRK1 and VARP. Nevertheless, the spacer could be replaced by GGGGS motifs of similar length rather than the original spacer (20 aa) without affecting neither LRRK1 nor VARP binding, indicating that its role is not sequence specific but only related to its length. We conclude that LRRK1 interacts with VAMP7 via the LD and that its binding to VAMP7 is more sensitive than that to VARP to the presence of the LD. The loss of mechano-sensing of exocytosis when the LD is removed thus likely results from the loss of a competition between LRRK1 and VARP. Furthermore, co-immunoprecipitation experiment showed that expression of the interaction domain (ID) of VARP, which mediates binding to VAMP7, competes with the binding of VAMP7 to VARP as expected and also the binding to LRRK1 (Figures 5E and 5F) to a similar extent (Tables S3 and S4). These data suggest that LRRK1 and VARP bind to VAMP7 via similar regions in ankyrin domains and likely compete for VAMP7 binding and/or generate mutually exclusive conformations of VAMP7. In good agreement with our hypothesis, triple labeling of exogenously expressed VAMP7, LRRK1, and VARP showed striking colocalization spots of VAMP7 and VARP in cell tips and colocalization spots of VAMP7 and LRRK1, without VARP, in the cell center (Figure 5G). GFP-LRRK1 and GFP-VARP but not soluble GFP showed significant colocalization with RFP-VAMP7 on Y patterns with enrichment of LRRK1 in cell center and VARP on cell tips (Figure S9). Altogether these data suggest that LRRK1 and VARP could compete for binding to VAMP7 and may have antagonistic functions in the intracellular distribution of VAMP7+ vesicles.

To further decipher the role of LRRK1, we silenced its expression by short hairpin RNA (shRNA) and assayed for VAMP7 exocytosis on soft and rigid substrate. We found that the exocytosis frequency of VAMP7 on soft substrate was increased to the same level as on rigid substrate in cells in which the expression of LRRK1 was knocked down (Figure 6A). Silencing of LRRK1 did not affect the persistence of VAMP7 pHluorin signal in the different stiffness conditions tested (Figure S7B), in good agreement with previous observations discussed earlier (Figure S7A). According to previous work on LRRK1, VAMP7-LRRK1 interaction should recruit CLIP-170 and dynein, allowing for retrograde transport on microtubules (Kedashiro et al., 2015a). To
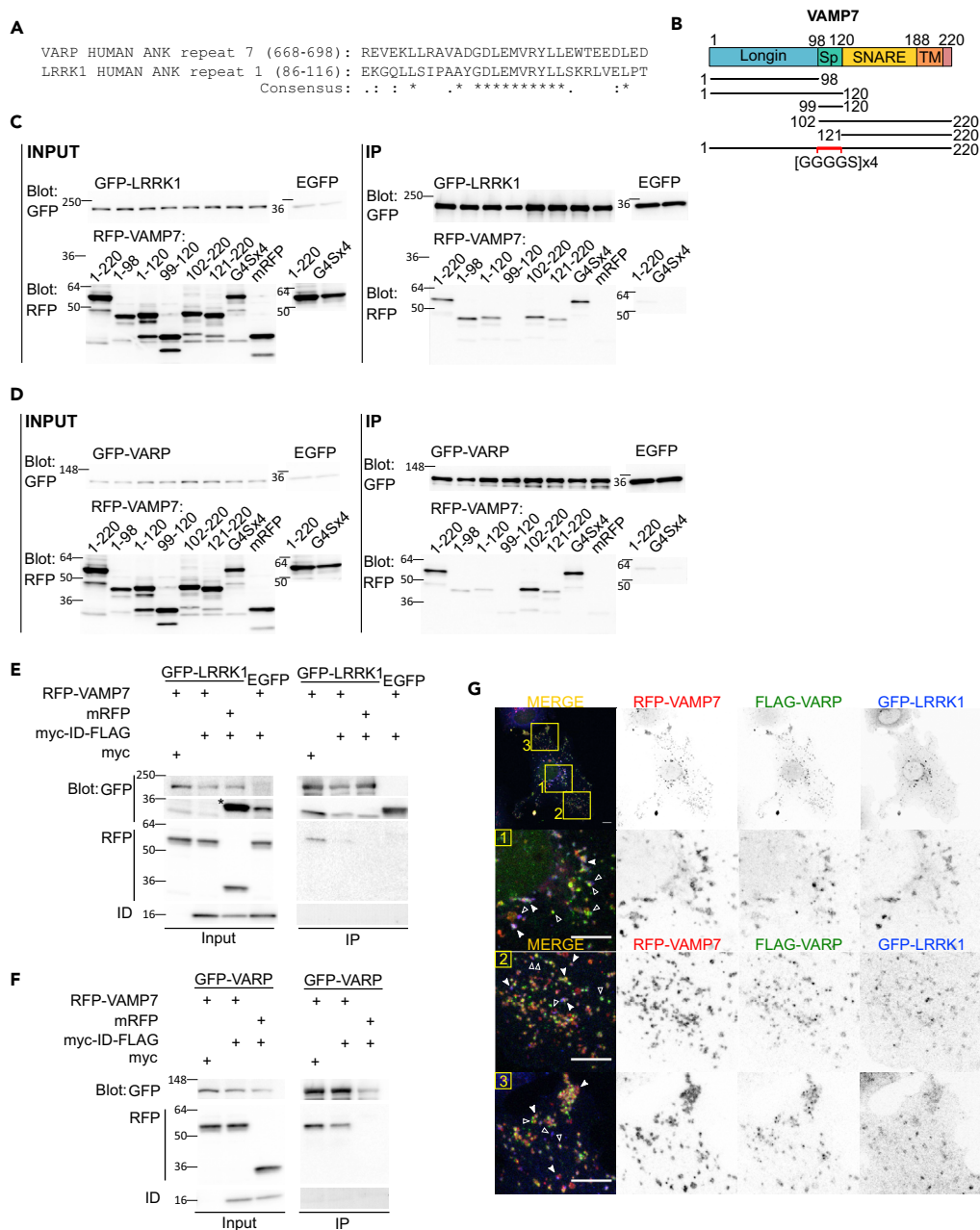
Figure 5. LRRK1 and VARP Compete for VAMP7 Binding

(A) Sequence alignment showing that LRRK1 shares a conserved ankyrin repeat domain with VARP in its interaction domain with VAMP7.

(B) Domain organization of rat VAMP7. Sp, spacer; TM, transmembrane. The constructs used for co-immunoprecipitation assay are shown below.

(C and D) Assays of binding of LRRK1 and VARP to VAMP7. Lysates from COS7 cells co-expressing GFP-LRRK1 or GFP-VARP with indicated RFP-tagged construction of VAMP7 were immunoprecipitated (IP) with GFP-binding protein (GBP) fixed on sepharose beads. Precipitated proteins were subjected to SDS-PAGE, and the blots were stained with antibodies against indicated target proteins. EGFP and monomeric RFP (mRFP) protein were used as control for nonspecific binding. The experiment has been independently repeated three times with similar results.

(E and F) Competition of VAMP7 interaction with LRRK1 and VARP by the VAMP7 interaction domain (ID) of VARP. Lysates from COS7 cells co-expressing indicated constructs were processed as described in (C) and (D). The expression of myc-ID-FLAG was detected by TG40, a rabbit polyclonal antibody raised against ID (Burgo et al., 2009).* previously revealed RFP signal. FLAG, epitope tag.

Figure 5. *Continued*

(G) Representative confocal microscopy sections of COS7 cell co-expressing RFP-VAMP7, FLAG-VARP, and GFP-LRRK1 grown on laminin-coated glass. Filled arrowheads indicate triple colocalization. Empty arrowheads indicate structures where either FLAG-VARP or GFP-LRRK1 is missing or dominant. Scale bar, 10 μm.

further understand the potential role of LRRK1 in VAMP7 trafficking, we carried out live imaging of cells expressing GFP-LRRK1 and RFP-VAMP7 and found that VAMP7 and LRRK1 accumulated together in the cell center upon epidermal growth factor (EGF) stimulation (Figures 6B and 6C), a condition that promotes perinuclear localization of LRRK1-containing endosomes (Hanafusa et al., 2011; Ishikawa et al., 2012). Analysis of confocal images taken from cells expressing GFP-tagged WT LRRK1, Y944F, or K1243M mutants (constitutively active and inactive kinase forms of LRRK1, respectively) and RFP-tagged VAMP7 showed that VAMP7 accumulated more in the perinuclear region in LRRK1 Y944F-expressing cells, and more toward the cell periphery in LRRK1 K1243M-expressing cells (Figures 7A and 7B), suggesting that LRRK1 kinase activity enhanced the retrograde transport of VAMP7 vesicles into the perinuclear region. We further immunoprecipitated GFP-tagged LRRK1 WT, Y944F, and K1243M mutants and assayed for coprecipitation of RFP-tagged VAMP7. We found that the kinase activity of LRRK1 is dispensable for its interaction with VAMP7 (Figure 7C and Table S5), in good agreement with the identification of the ID in the amino-terminal domain of LRRK1 as previously shown (Toyofuku et al., 2015). LRRK1 was previously found to play a role in autophagy (Toyofuku et al., 2015), but we did not find significant autophagy induction as seen by LC3-II imaging in cells on soft versus rigid substrates and western blotting (Figure S10). We conclude that LRRK1 mediates retrograde transport of VAMP7 in a kinase-dependent activity and that LRRK1 is required for the control of VAMP7 exocytosis in response to substrate rigidity.

Opposite Roles of LRRK1 and VARP in Mechanosensing

A prediction from our previous results showing that VAMP7 exocytosis is involved in mechanosensing (Figure 1), and that LRRK1 and VARP compete for binding to VAMP7 (Figure 5), would be that LRRK1 and VARP could generate a tug-of-war mechanism for the cell positioning of secretory lysosomes in the context of mechanosensing. To test this hypothesis, we again used the previous assay with cells grown on substrates of different rigidities. We found that soft substrate promoted more perinuclear accumulation of VAMP7 than rigid substrate (Figures 8A and 8B), similar to the effect of LRRK1 Y944F mutant (Figures 7A and 7B). We found that VAMP7 was localized more to the center in LRRK1-overexpressing cells. The opposite result was found in VARP-overexpressing cells, which showed decreased center-localized VAMP7. VARP-overexpressing cells further display striking concentration of VAMP7 at the tips of cell protrusions. The effects of WT LRRK1 and VARP overexpression were not sensitive to substrate rigidity. These later data suggest that the effect of overexpression of these proteins dominated over the regulation that occurs between soft and rigid environment when they are expressed at physiological levels. To further decipher the role of VARP and LRRK1, we then used the Crispr/Cas9 approach to knock out the expression of the proteins (Figure S1A), cultured the KO cells on substrate of 1.5 and 28 kPa, and assayed for perinuclear accumulation of RFP-VAMP7 (Figures 8C and 8D). We again reproduced the decreased perinuclear concentration of VAMP7 on more rigid substrate in control cells. The effect of rigidity was lost in LRRK1 KO cells. On the contrary, re-expression of LRRK1 in KO cells exacerbated central concentration of VAMP7. Conversely, VARP KO showed strong perinuclear accumulation of VAMP7 on rigid substrate, and this effect was rescued by the re-expression of VARP. In this later case, the effect of substrate rigidity was clearly visible after VARP re-expression in VARP KO cells. The KOs of VARP and LRRK1 did not lead to strong variations of microtubules (Figure S11) and MLC2 subcellular localization (Figure S5B).

Interestingly, expression of a point mutant of VARP (the so-called DADA mutant) unable to bind VAMP7 (Schäfer et al., 2012) was unable to rescue the phenotype of VARP KO cells on 28-kPa rigid substrate, whereas, as expected, the WT form of VARP fully rescued the subcellular localization of VAMP7 in the cell periphery on rigid substrate (Figures 8E and 8F). In the rescue conditions, exogenous VARP and LRRK1 partially colocalized with VAMP7 (Figure S9). Altogether, these experiments using KO, rescue, and overexpression approaches and culture on soft and rigid substrate suggest that LRRK1 and VARP provides a tug-of-war mechanism, which mediates the fine-tuning of VAMP7 subcellular localization regulated by substrate rigidity (Figure 9). In this regulatory mechanism, the precise expression level of LRRK1 and VARP appeared to be a critical parameter, further reinforcing the notion of a competitive mechanism strongly dependent on the concentration and activity of LRRK1 and VARP.
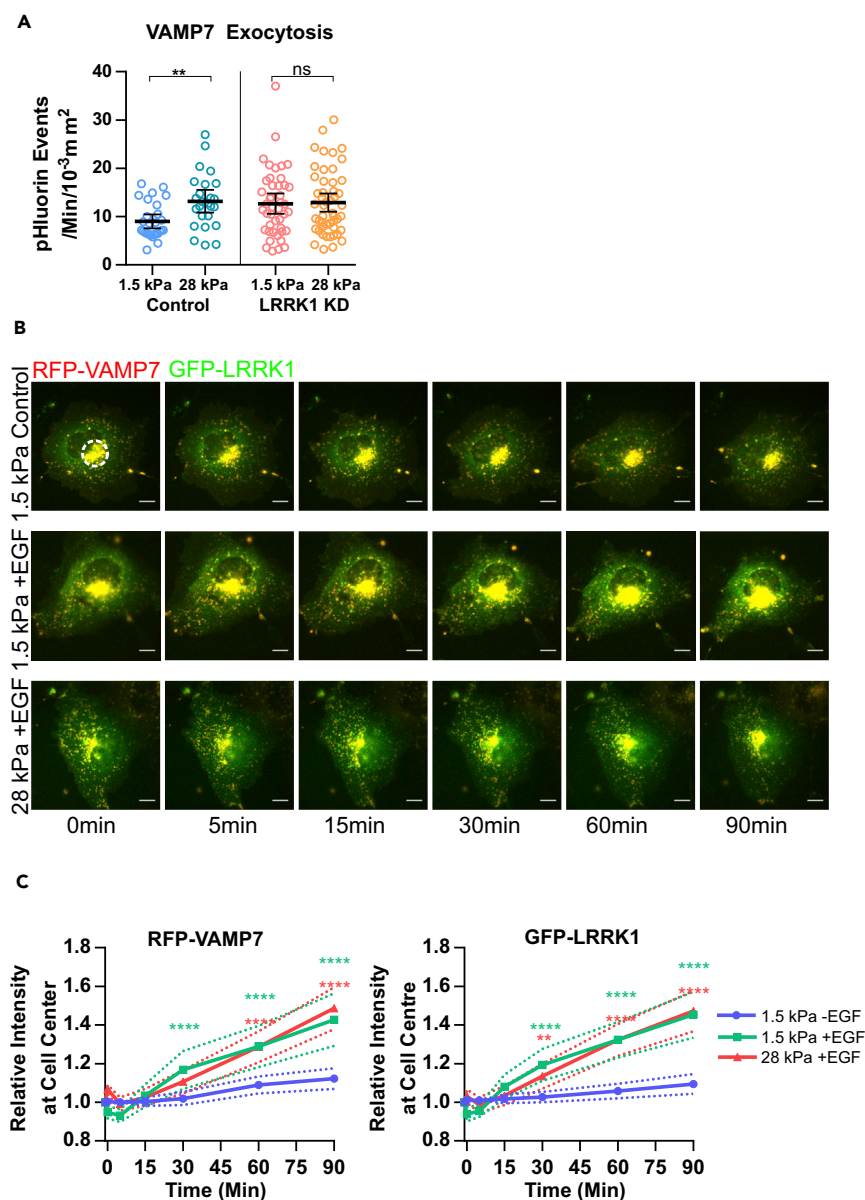
A

VAMP7 Exocytosis

B

RFP-VAMP7 GFP-LRRK1

0min   5min   15min   30min   60min   90min

C

Figure 6. LRRK1 Regulates VAMP7 Trafficking and Mechanosensing

(A) Quantification of exocytic events in COS7 cells co-expressing VAMP7-pHluorin with control shRNA or LRRK1-shRNA, grown on laminin-coated PDMS gels for 18–24 hr. Graph shows scatterplot with mean ± 95% confidence interval (CI). Each point represents the exocytic rate of cells from two independent experiments. n = 51, 62, 57, and 53 cells, respectively. **p < 0.01, Welsh's t test.

(B) VAMP7 and LRRK1 accumulated together in perinuclear endosomes upon EGF stimulation. COS7 cells co-expressing RFP-VAMP7 and GFP-LRRK1 were imaged by wide field microscopy 24 hr after plating on laminin-coated 1.5- or 28-kPa PDMS gel. EGF was injected into the imaging chamber between minutes −1 and 0 to a final concentration of 100 ng/mL. Scale bar: 10 μm.

(C) Quantification of the accumulation of fluorescence signal at the cell center. The cell center was defined by calculating the local center of mass using an ImageJ script. The total fluorescence intensity was measured inside a 16-μm-diameter oval around the cell center (dashed circle in Figure 6B) and compared with the total fluorescence intensity outside the circle. 1.5 kPa - EGF n = 54, 1.5 kPa + EGF n = 39, 28 kPa + EGF n = 51. Data were pooled from two independent experiments. Graph shows mean with 95% CI (dotted lines). **p < 0.01, ****p < 0.0001, ANOVA with Tukey's post hoc.
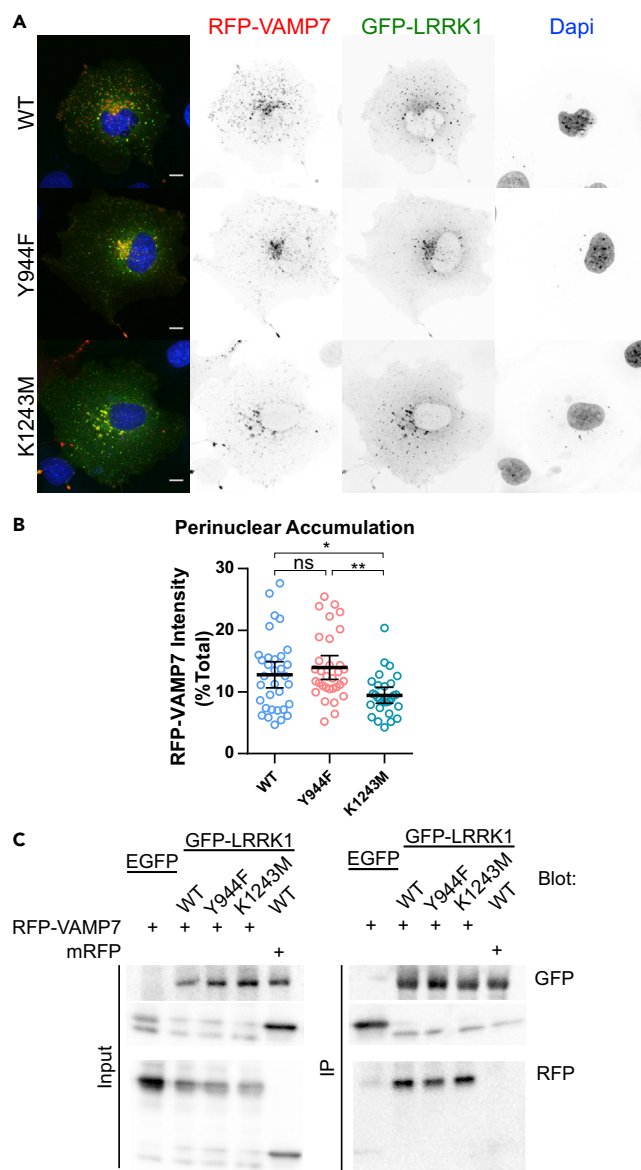
Figure 7. LRRK1 Kinase Activity Regulates VAMP7 Retrograde Transport

(A) Representative projection of confocal microscopy optical sections of COS7 cells co-expressing RFP-VAMP7 with GFP-tagged WT LRRK1, Y944F (kinase constitutively active), and K1243M (kinase dead) mutants grown on laminin-coated glass coverslips for 18–24 hr. Images show z-projection of confocal stack. Scale bar: 10 μm.

(B) Quantification of the accumulation of RFP-VAMP7 fluorescence signal at the cell center. The cell center was defined by calculating the local center of mass using an ImageJ script. The fluorescence intensity was measured inside a 10-μm-diameter oval around the cell center and reported to the total fluorescence intensity. Each point represents the data measured from cells from two independent experiments. Graph shows mean with 95% confidence interval (CI). n = 33, 32, and 29 cells, respectively. *p < 0.05, **p < 0.01; ANOVA with Tukey's post hoc. ns, not significant.

(C) Assays of binding of VAMP7 to WT, Y944F, and K1243M LRRK1. Lysates from COS7 cells co-expressing RFP-VAMP7 with indicated GFP-tagged construction of LRRK1 were immunoprecipitated (IP) with GFP-binding protein (GBP) fixed on sepharose beads. Precipitated proteins were subjected to SDS-PAGE, and the blots were stained with antibodies against indicated target proteins. EGFP and mRFP protein were used as control for nonspecific binding. The experiment has been independently repeated three times with similar results.
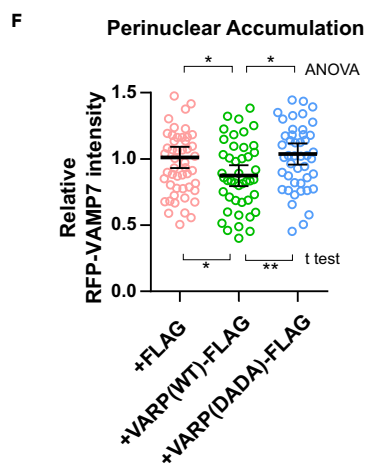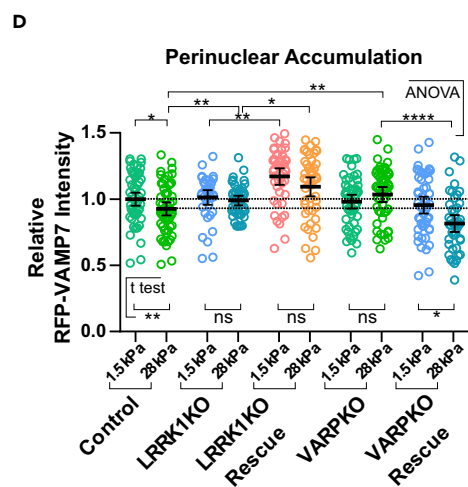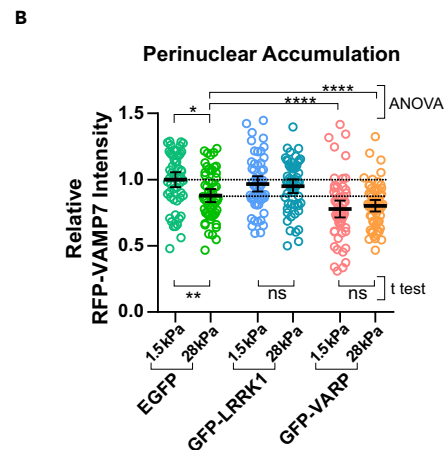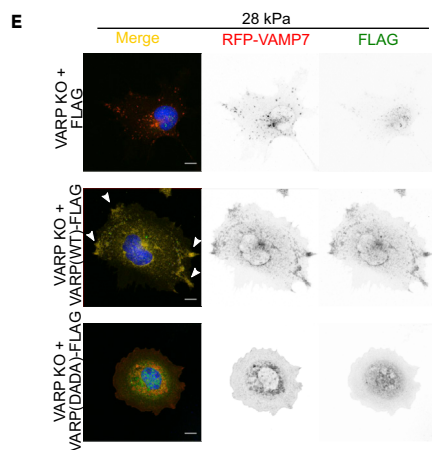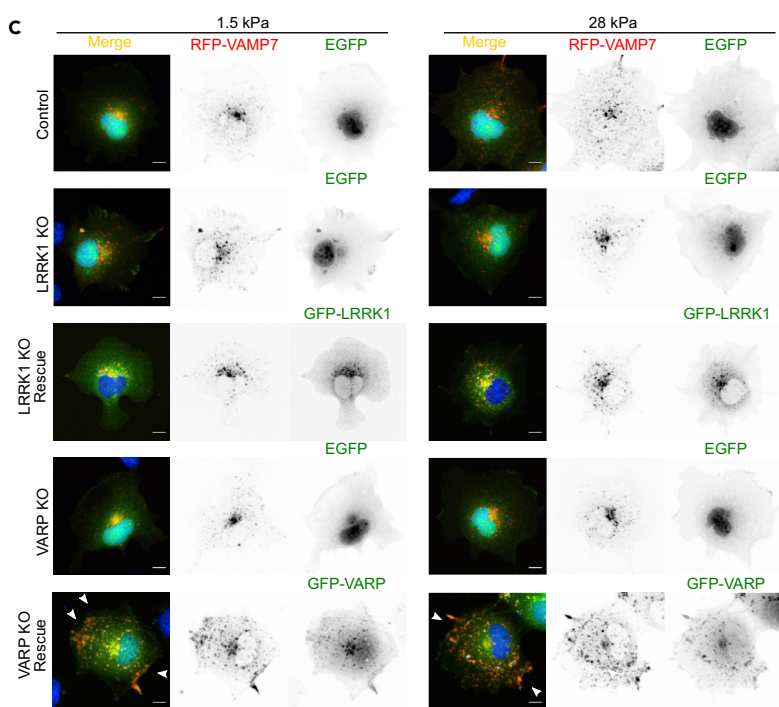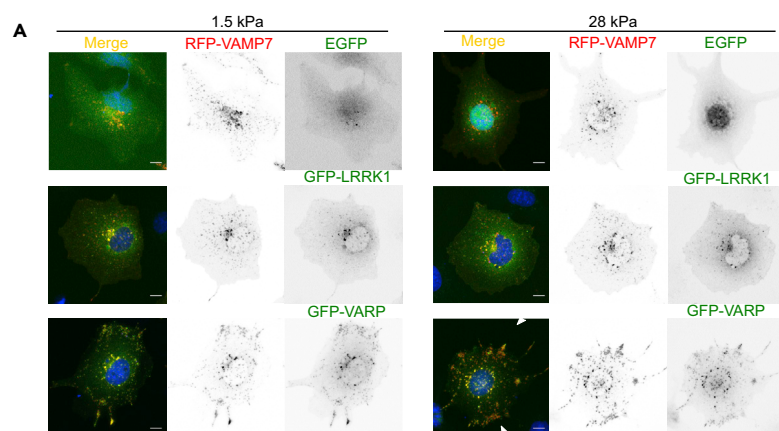
Figure 8. LRRK1 and VARP Have Opposite Roles in Rigidity-Dependent VAMP7 Positioning

(A) Representative WT COS7 cells co-expressing RFP-tagged VAMP7 with GFP-tagged LRRK1 or VARP, grown on laminin-coated PDMS gels. Images show z-projection of confocal stack. Arrowheads show the colocalization in cell protrusions. Scale bar: 10 μm.

(C) Representative control, LRRK1 KO, and VARP KO COS7 cells grown on laminin-coated PDMS gels. Control and KO cells were transfected with RFP-VAMP7 and EGFP as indicated, and with GFP-LRRK1 and VARP in rescue conditions. Images show z-projection of confocal stack. Arrowheads show the colocalization in cell protrusions. Scale bar: 10 μm.

(E) Representative VARP KO cells expressing FLAG tag, FLAG-tagged wild-type VARP, and FLAG-tagged VARP with DADA mutation and grown on laminin-coated 28-kPa PDMS gels. Images show z-projection of confocal stack. Arrowheads show the colocalization in cell protrusions. Scale bar: 10 μm. Note the rescue by wild-type but not DADA mutant of VARP.

(B, D, and F) Quantification of RFP-VAMP7 fluorescence in the perinuclear region. Graph shows scatterplot with mean ± 95% confidence interval (CI). Each point represents the value obtained from a cell pooled from two independent experiments. (B) n = 55, 53, 52, 55, 56, and 58; (D) n = 57, 57, 39, 44, 45, 45, 50, 51, 51, and 44; (F) n = 53, 44, and 47 cells, respectively. *p < 0.05, **p < 0.01, and ****p < 0.0001, ANOVA with Tukey's post hoc or Welsh's t test was used as indicated.

DISCUSSION

In this study, we found that VAMP7-dependent lysosomal exocytosis was required for cells to sense substrate rigidity and that the latter redistributed VAMP7 to the cell periphery in an LD-, VARP-, and LRRK1-dependent manner. LRRK1 and VARP appeared to compete for VAMP7 binding via a conserved domain in one of their ankyrin repeats and operate via opposite control of the availability for secretion of peripheral VAMP7 vesicles in response to mechanical constraints, thus suggesting a tug-of-war mechanism.

VAMP7 KO COS7 cells showed remarkably increased cell elasticity on soft substrate and decreased elasticity on more rigid substrate compared with control cells. This likely suggests that the lack of VAMP7 may prevent cells from properly responding to mechanical constraints. Conversely, substrate rigidity increased exocytosis of VAMP7, but not VAMP2. This likely indicates the need for different types of membranes being transported to the cell surface depending on the biophysical properties of cell environment, particularly its rigidity. VAMP7 was shown to be important for phagophore formation and autophagosome secretion (Fader et al., 2012; Moreau et al., 2011) and rigidity was shown to increase autophagy (Ulbricht et al., 2013), but we did not find significant LC3-II induction in the different conditions tested, so we do not think that substrate stiffness significantly activated autophagy in our experimental conditions.

Cell tension is the combination of two factors: the cortical tension of actomyosin cytoskeleton and the in-plane tension of plasma membrane (Sens and Plastino, 2015). We found that hyper-osmotic shock inhibited the exocytosis frequency of VAMP7 following a remarkably quick adaptation of exocytosis frequency to strong changes in membrane tension. The effect of hyper-osmotic shock on persistence of the signal at plasma membrane would be best explained by decreased fusion pore flattening because fusion pore growth is promoted or even driven by the membrane tension (Bretou et al., 2014) and potential increased recovery of plasma membrane by endocytosis upon the osmotic shock. Our data thus fit well with the notion that exocytosis increases the surface area and therefore decreases membrane tension, and thus needs to be shut down to compensate for decreased membrane tension following hyper-osmotic shock (Gauthier et al., 2011; Keren, 2011; Sens and Plastino, 2015). Nevertheless, we found similar effects of hyper-osmotic shock on VAMP7 deleted of its LD, whereas this was not the case for increased substrate stiffness. This indicates that acute changes of cell tension, such as osmotic shocks, acting likely via a direct effect on membrane tension, and secretory vesicles in close proximity with the plasma membrane, proceed through mechanisms different from substrate stiffness. Altogether, our results suggest that of the two components of cell tension (membrane tension and cortical tension), the first may operate in the context of hyper-osmotic shock and not be specific of VAMP7 because it was Longin independent (Figures 4C and 4D), whereas the latter may be the main regulation that is activated by substrate rigidity in the presence of laminin (Figure 3).

It is intriguing that substrate rigidity and composition affected exocytosis of VAMP7, i.e., late endosomal and lysosomal CD63+ exocytosis but not VAMP2, i.e., fast endosomal recycling. This likely indicates the need for different types of membranes being transported to the cell surface depending on the cell environment. We think that our findings are related to the previous demonstration that VAMP7 mediates the transport of GPI-anchored proteins and lipid microdomains to the plasma membrane (Lafont et al., 1999; Molino et al., 2015; Pocard et al., 2007), which in turn modulates integrin dynamics and adhesion (Eich et al., 2016; van Zanten et al., 2009), epidermal growth factor (EGFR)-containing microdomains,
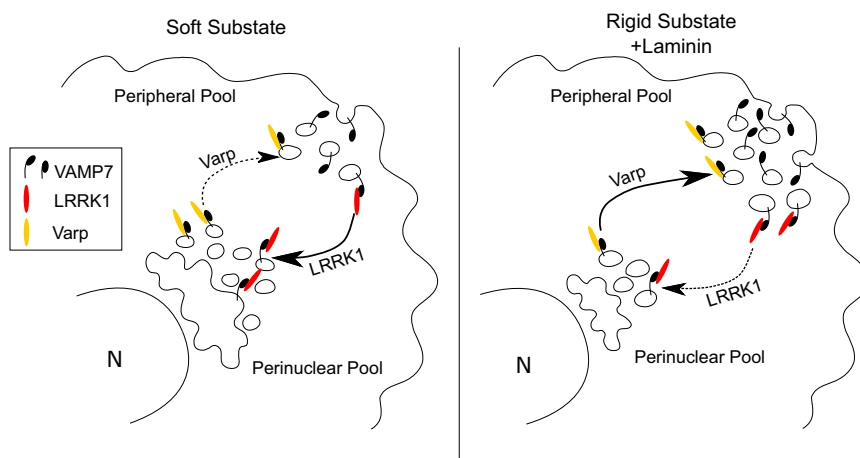
Figure 9. Hypothetical Working Model

Working hypothesis describing a tug-of-war mechanism with LRRK1 on the retrograde end and Varp on the anterograde end of VAMP7 transport. On the soft substrate, high activity of LRRK1 and low activity of VARP favors the retrograde transport of VAMP7 vesicles, and as a result, depletes the availability of peripheral VAMP7 pool. On the rigid substrate, weaker activity of LRRK1 and stronger activity of VARP increase the amount of VAMP7 vesicles in the periphery.

and EGF signaling (Danglot et al., 2010). Accordingly, increased exocytosis of GPI-anchored proteins was found in the secondary contractile phase during cell spreading (Gauthier et al., 2011). An attractive hypothesis would be that VAMP7+/CD63+ secretory late endosomes and lysosomes bring to the plasma membrane lipids that best fit a membrane under tension such as on more rigid substrates and more general transport membrane microdomains, which are important for cells to regulate their biomechanical properties and sense substrate rigidity. Further studies are now required to decipher the precise signaling mechanism from rigidity sensing and cortical tension all the way down to VAMP7 exocytosis.

The mechanism unraveled here further suggests the involvement of two members of VAMP7's hub in mechanosensing-dependent regulation of transport and exocytosis (see working hypothesis model in Figure 8). Here we found that LRRK1 strongly interacts with LD and SNARE domain of VAMP7 with a particularly strong interaction with LD *in vitro*. LRRK1 and VAMP7 were co-transported to the cell center upon EGF addition. Silencing LRRK1 removed the regulation of VAMP7 exocytosis by substrate rigidity. LRRK1 overexpression concentrated VAMP7 in the cell center. This effect dominated over substrate rigidity and was further emphasized by kinase activity, as it was previously shown in the case of the EGFR (Ishikawa et al., 2012). VARP mediates transport of VAMP7 to the cell periphery (Burgo et al., 2009, 2012; Hesketh et al., 2014). Here we found that VARP bound efficiently ΔLD VAMP7 and its overexpression decreased the perinuclear pool of VAMP7 while increasing the peripheral one. Our data thus give a reasonable explanation for the increased exocytosis frequency of ΔLD VAMP7, as the latter would still efficiently bind to VARP and less to LRRK1. VARP interacts with the retromer and kinesin 1, and these interactions are important for the transport of VAMP7 toward the cell periphery on microtubules (Burgo et al., 2009, 2012; Hesketh et al., 2014; Schäfer et al., 2012). Conversely, LRRK1 interacts with the dynein complex, which mediates retrograde transport on microtubules toward the cell center (Kedashiro et al., 2015b). In addition, the movement of lysosomes toward the peripheral cytoplasm depends on the BORC/BLOC-mediated coupling to microtubule plus end-directed kinesin motors (Dennis et al., 2016; Guardia et al., 2016; Pu et al., 2015). In addition, a recent article found that Rab3 and its effector myosin IIA play an important role in the transport to the periphery and secretion of lysosomes (Encarnação et al., 2016). Here we have used COS7 cells, which were shown to lack myosin IIA (Even-Ram et al., 2007). Thus future studies should address the potential cross talk between the VARP-LRKK1 tug-of-war mechanism unraveled here, likely connected to motility on microtubules, and the one involving myosin IIA (Encarnação et al., 2016), and possibly the retromer-associated WASH complex recruited by VARP (Hesketh et al., 2014; McGough et al., 2014) and motility of lysosomes on actin microfilaments. Future studies should certainly address the potential regulation of these interactions by substrate rigidity sensing and signaling.

Altogether, the present data lead us to propose a tug-of-war molecular mechanism with LRRK1 and VARP competing for VAMP7 binding, LRRK1 acting on the retrograde end and VARP on the anterograde end of VAMP7 trafficking. Our results further suggest that substrate stiffness would be able to regulate the tug-of-war between LRRK1 and VARP for lysosome positioning in the cell periphery and exocytosis. The effects of LRRK1 and VARP suggest that their concentration in the cell is important for VAMP7 center to periphery distribution, fitting well with the notion of a tug-of-war mechanism. The signaling pathways that may regulate the expression of LRRK1 and VARP will also require further investigation as our data suggest that the relative amounts of these proteins are important for secretory lysosome positioning. Interestingly, VARP binds Rab40C and this protein promotes proteasomal degradation of VARP (Yatsu et al., 2015), and RACK1 inhibits the interaction between Varp and Rab40C, thus counteracting the negative effect of Rab40C (Marubashi et al., 2016). RACK1 is downstream of β1 integrin (Lee et al., 2002; Liliental and Chang, 1998) and IGFR1 (Kiely et al., 2002; Zhang et al., 2006), which has been shown to activate VAMP7 exocytosis (Burgo et al., 2013). Thus it is tempting to speculate that the turnover of VARP may be regulated by integrin-dependent mechanosensing, a hypothesis that will now require investigation.

In conclusion, we suggest that VAMP7 lysosomal secretion is regulated by biomechanical constraints relayed by LRRK1 and VARP (Figure 9), a mechanism with potential broad relevance for plasma membrane dynamics in normal conditions (Koseoglu et al., 2015), infection (Chiaruttini et al., 2016; Larghi et al., 2013), stem cell differentiation (Engler et al., 2006), and cancer (Kostic et al., 2009; Steffen et al., 2008), which all were shown to be linked to mechanical constraints.

METHODS

All methods can be found in the accompanying Transparent Methods supplemental file.

SUPPLEMENTAL INFORMATION

Supplemental Information includes Transparent Methods, 11 figures, 5 tables, and 3 videos and can be found with this article online at https://doi.org/10.1016/j.isci.2018.05.016.

AUTHOR CONTRIBUTIONS

Conceptualization, G.W. and T.G.; Methodology, G.W., S.B., and S.N.; Software, G.W.; Investigation, G.W., S.N., S.B., and P.B.; Writing – Original Draft, G.W. and T.G.; Funding Acquisition, G.W. and T.G.; Supervision, T.G., F.L., and M.C.-M.

DECLARATION OF INTERESTS

The authors declare no competing interests.

REFERENCES

Albert, P.J., and Schwarz, U.S. (2014). Dynamics of cell shape and forces on micropatterned substrates predicted by a cellular Potts model. Biophys. J. *106*, 2340–2352.

Balaji, J., and Ryan, T.A. (2007). Single-vesicle imaging reveals that synaptic vesicle exocytosis and endocytosis are coupled by a single stochastic mode. Proc. Natl. Acad. Sci. USA *104*, 20576–20581.

Bretou, M., Jouannot, O., Fanget, I., Pierobon, P., Larochette, N., Gestraud, P., Guillon, M., Emiliani, V., Gasman, S., Desnos, C., et al. (2014). Cdc42 controls the dilation of the exocytotic fusion pore by regulating membrane tension. Mol. Biol. Cell *25*, 3195–3209.

Burgo, A., Sotirakis, E., Simmler, M.-C., Verraes, A., Chamot, C., Simpson, J.C., Lanzetti, L., Proux-Gillardeaux, V., and Galli, T. (2009). Role of Varp, a Rab21 exchange factor and TI-VAMP/VAMP7 partner, in neurite growth. EMBO Rep. *10*, 1117–1124.

Burgo, A., Proux-Gillardeaux, V., Sotirakis, E., Bun, P., Casano, A., Verraes, A., Liem, R.K.H., Formstecher, E., Coppey-Moisan, M., and Galli, T. (2012). A molecular network for the transport of the TI-VAMP/VAMP7 vesicles from cell center to periphery. Dev. Cell *23*, 166–180.

Burgo, A., Casano, A.M., Kuster, A., Arold, S.T., Wang, G., Nola, S., Verraes, A., Dingli, F., Loew, D., and Galli, T. (2013). Increased activity of the vesicular soluble N-ethylmaleimide-sensitive factor attachment protein receptor TI-VAMP/VAMP7 by tyrosine phosphorylation in the Longin domain. J. Biol. Chem. *288*, 11960–11972.

Chen, B., Ji, B., and Gao, H. (2015). Modeling active mechanosensing in cell-matrix interactions. Annu. Rev. Biophys. *44*, 1–32.

Chiaruttini, G., Piperno, G.M., Jouve, M., De Nardi, F., Larghi, P., Peden, A.A., Baj, G., Müller, S., Valitutti, S., Galli, T., et al. (2016). The SNARE VAMP7 regulates exocytic trafficking of interleukin-12 in dendritic cells. Cell Rep. *14*, 2624–2636.

Coco, S., Raposo, G., Martinez, S., Fontaine, J.J., Takamori, S., Zahraoui, A., Jahn, R., Matteoli, M., Louvard, D., and Galli, T. (1999). Subcellular localization of tetanus neurotoxin-insensitive vesicle-associated membrane protein (VAMP)/VAMP7 in neuronal cells: evidence for a novel membrane compartment. J. Neurosci. *19*, 9803–9812.

Danglot, L., Chaineau, M., Dahan, M., Gendron, M.-C., Boggetto, N., Perez, F., and Galli, T. (2010). Role of TI-VAMP and CD82 in EGFR cell-surface dynamics and signaling. J. Cell Sci. *123*, 723–735.

Daste, F., Galli, T., and Tareste, D. (2015). Structure and function of longin SNAREs. J. Cell Sci. *128*, 4263–4272.

Dennis, M.K., Delevoye, C., Acosta-Ruiz, A., Hurbain, I., Romao, M., Hesketh, G.G., Goff, P.S., Sviderskaya, E.V., Bennett, D.C., Luzio, J.P., et al. (2016). BLOC-1 and BLOC-3 regulate VAMP7 cycling to and from melanosomes via distinct tubular transport carriers. J. Cell Biol. *214*, 293–308.

Eich, C., Manzo, C., de Keijzer, S., Bakker, G.-J., Reinieren-Beeren, I., García-Parajo, M.F., and Cambi, A. (2016). Changes in membrane sphingolipid composition modulate dynamics and adhesion of integrin nanoclusters. Sci. Rep. *6*, 20693.

Encarnação, M., Espada, L., Escrevente, C., Mateus, D., Ramalho, J., Michelet, X., Santarino, I., Hsu, V.W., Brenner, M.B., Barral, D.C., et al. (2016). A Rab3a-dependent complex essential for lysosome positioning and plasma membrane repair. J. Cell Biol. *213*, 631–640.

Engler, A.J., Sen, S., Sweeney, H.L., and Discher, D.E. (2006). Matrix elasticity directs stem cell lineage specification. Cell *126*, 677–689.

Even-Ram, S., Doyle, A.D., Conti, M.A., Matsumoto, K., Adelstein, R.S., and Yamada, K.M. (2007). Myosin IIA regulates cell motility and actomyosin-microtubule crosstalk. Nat. Cell Biol *9*, 299–309.

Fader, C.M., Aguilera, M.O., and Colombo, M.I. (2012). ATP is released from autophagic vesicles to the extracellular space in a VAMP7-dependent manner. Autophagy *8*, 1741–1756.

Gauthier, N.C., Fardin, M.A., Roca-Cusachs, P., and Sheetz, M.P. (2011). Temporary increase in plasma membrane tension coordinates the activation of exocytosis and contraction during cell spreading. Proc. Natl. Acad. Sci. USA *108*, 14467–14472.

Ghosh, D., Pinto, S., Danglot, L., Vandewauw, I., Segal, A., Van Ranst, N., Benoit, M., Janssens, A., Vennekens, R., Vanden Berghe, P., et al. (2016). VAMP7 regulates constitutive membrane incorporation of the cold-activated channel TRPM8. Nat. Commun. *7*, 10489.

Guardia, C.M., Farías, G.G., Jia, R., Pu, J., and Bonifacino, J.S. (2016). BORC functions upstream of kinesins 1 and 3 to coordinate regional movement of lysosomes along different microtubule tracks. Cell Rep. *17*, 1950–1961.

Gupton, S.L., and Gertler, F.B. (2010). Integrin signaling switches the cytoskeletal and exocytic machinery that drives neuritogenesis. Dev. Cell *18*, 725–736.

Hämälistö, S., and Jäättelä, M. (2016). Lysosomes in cancer-living on the edge (of the cell). Curr. Opin. Cell Biol. *39*, 69–76.

Hanafusa, H., Ishikawa, K., Kedashiro, S., Saigo, T., Iemura, S.-I., Natsume, T., Komada, M., Shibuya, H., Nara, A., and Matsumoto, K. (2011). Leucine-rich repeat kinase LRRK1 regulates endosomal trafficking of the EGF receptor. Nat. Commun. *2*, 158.

Hasan, N., and Hu, C. (2010). Vesicle-associated membrane protein 2 mediates trafficking of alpha5beta1 integrin to the plasma membrane. Exp. Cell Res. *316*, 12–23.

Hesketh, G.G., Pérez-Dorado, I., Jackson, L.P., Wartosch, L., Schäfer, I.B., Gray, S.R., McCoy, A.J., Zeldin, O.B., Garman, E.F., Harbour, M.E., et al. (2014). VARP is recruited on to endosomes by direct interaction with retromer, where together they function in export to the cell surface. Dev. Cell *29*, 591–606.

Ishikawa, K., Nara, A., Matsumoto, K., and Hanafusa, H. (2012). EGFR-dependent phosphorylation of leucine-rich repeat kinase LRRK1 is important for proper endosomal trafficking of EGFR. Mol. Biol. Cell *23*, 1294–1306.

Jaiswal, J.K., Andrews, N.W., and Simon, S.M. (2002). Membrane proximal lysosomes are the major vesicles responsible for calcium-dependent exocytosis in nonsecretory cells. J. Cell Biol. *159*, 625–635.

Kedashiro, S., Pastuhov, S.I., Nishioka, T., Watanabe, T., Kaibuchi, K., Matsumoto, K., and Hanafusa, H. (2015a). LRRK1-phosphorylated CLIP-170 regulates EGFR trafficking by recruiting p150Glued to microtubule plus ends. J. Cell Sci. *128*, 385–396.

Kedashiro, S., Pastuhov, S.I., Nishioka, T., Watanabe, T., Kaibuchi, K., Matsumoto, K., and Hanafusa, H. (2015b). LRRK1-phosphorylated CLIP-170 regulates EGFR trafficking by recruiting p150Glued to microtubule plus ends. J. Cell Sci. *128*, 829.

Kent, H.M., Evans, P.R., Schäfer, I.B., Gray, S.R., Sanderson, C.M., Luzio, J.P., Peden, A.A., and Owen, D.J. (2012). Structural basis of the intracellular sorting of the SNARE VAMP7 by the AP3 adaptor complex. Dev. Cell *22*, 979–988.

Keren, K. (2011). Membrane tension leads the way. Proc. Natl. Acad. Sci. USA *108*, 14379–14380.

Kiely, P.A., Sant, A., and O'Connor, R. (2002). RACK1 is an insulin-like growth factor 1 (IGF-1) receptor-interacting protein that can regulate IGF-1-mediated Akt activation and protection from cell death. J. Biol. Chem. *277*, 22581–22589.

Koseoglu, S., Peters, C.G., Fitch-Tewfik, J.L., Aisiku, O., Danglot, L., Galli, T., and Flaumenhaft, R. (2015). VAMP-7 links granule exocytosis to actin reorganization during platelet activation. Blood *126*, 651–660.

Kostic, A., Lynch, C.D., and Sheetz, M.P. (2009). Differential matrix rigidity response in breast cancer cell lines correlates with the tissue tropism. PLoS One *4*, e6361.

Lafont, F., Verkade, P., Galli, T., Wimmer, C., Louvard, D., and Simons, K. (1999). Raft association of SNAP receptors acting in apical trafficking in Madin-Darby canine kidney cells. Proc. Natl. Acad. Sci. USA *96*, 3734–3738.

Larghi, P., Williamson, D.J., Carpier, J.-M., Dogniaux, S., Chemin, K., Bohineust, A., Danglot, L., Gaus, K., Galli, T., and Hivroz, C. (2013). VAMP7 controls T cell activation by regulating the recruitment and phosphorylation of vesicular Lat at TCR-activation sites. Nat. Immunol. *14*, 723–731.

Lee, H.S., Millward-Sadler, S.J., Wright, M.O., Nuki, G., Al-Jamal, R., and Salter, D.M. (2002). Activation of Integrin-RACK1/PKC alpha signalling in human articular chondrocyte mechanotransduction. Osteoarthritis Cartilage *10*, 890–897.

Li, D., Ropert, N., Koulakoff, A., Giaume, C., and Oheim, M. (2008). Lysosomes are the major vesicular compartment undergoing

Ca2+-regulated exocytosis from cortical astrocytes. J. Neurosci. *28*, 7648–7658.

Liliental, J., and Chang, D.D. (1998). Rack1, a receptor for activated protein kinase C, interacts with integrin beta subunit. J. Biol. Chem. *273*, 2379–2383.

Martinez-Arca, S., Coco, S., Mainguy, G., Schenk, U., Alberts, P., Bouillé, P., Mezzina, M., Prochiantz, A., Matteoli, M., Louvard, D., et al. (2001). A common exocytotic mechanism mediates axonal and dendritic outgrowth. J. Neurosci. *21*, 3830–3838.

Martinez-Arca, S., Rudge, R., Vacca, M., Raposo, G., Camonis, J., Proux-Gillardeaux, V., Daviet, L., Formstecher, E., Hamburger, A., Filippini, F., et al. (2003). A dual mechanism controlling the localization and function of exocytic v-SNAREs. Proc. Natl. Acad. Sci. USA *100*, 9011–9016.

Marubashi, S., Ohbayashi, N., and Fukuda, M. (2016). A varp-binding protein, RACK1, regulates dendrite outgrowth through stabilization of varp protein in mouse melanocytes. J. Invest Dermatol. *136*, 1672–1680.

McGough, I.J., Steinberg, F., Gallon, M., Yatsu, A., Ohbayashi, N., Heesom, K.J., Fukuda, M., and Cullen, P.J. (2014). Identification of molecular heterogeneity in SNX27-retromer-mediated endosome-to-plasma-membrane recycling. J. Cell Sci. *127*, 4940–4953.

Messica, Y., Laser-Azogui, A., Volberg, T., Elisha, Y., Lysakovskaia, K., Eils, R., Gladilin, E., Geiger, B., and Beck, R. (2017). The role of vimentin in regulating cell invasive migration in dense cultures of breast carcinoma cells. Nano Lett. *17*, 6941–6948.

Molino, D., Nola, S., Lam, S.M., Verraes, A., Proux-Gillardeaux, V., Boncompain, G., Perez, F., Wenk, M., Shui, G., Danglot, L., et al. (2015). Role of tetanus neurotoxin insensitive vesicle-associated membrane protein in membrane domains transport and homeostasis. Cell Logist *5*, e1025182.

Moreau, K., Ravikumar, B., Renna, M., Puri, C., and Rubinsztein, D.C. (2011). Autophagosome precursor maturation requires homotypic fusion. Cell *146*, 303–317.

Niessen, C.M., Hulsman, E.H., Rots, E.S., Sánchez-Aparicio, P., and Sonnenberg, A. (1997). Integrin alpha 6 beta 4 forms a complex with the cytoskeletal protein HD1 and induces its redistribution in transfected COS-7 cells. Mol. Biol. Cell *8*, 555–566.

Papadopulos, A., Gomez, G.A., Martin, S., Jackson, J., Gormal, R.S., Keating, D.J., Yap, A.S., and Meunier, F.A. (2015). Activity-driven relaxation of the cortical actomyosin II network synchronizes Munc18-1-dependent neurosecretory vesicle docking. Nat. Commun. *6*, 6297.

Parsons, J.T., Horwitz, A.R., and Schwartz, M.A. (2010). Cell adhesion: integrating cytoskeletal dynamics and cellular tension. Nat. Rev. Mol. Cell Biol. *11*, 633–643.

Pocard, T., Le Bivic, A., Galli, T., and Zurzolo, C. (2007). Distinct v-SNAREs regulate direct and indirect apical delivery in polarized epithelial cells. J. Cell Sci. *120*, 3309–3320.

Proux-Gillardeaux, V., Rudge, R., and Galli, T. (2005a). The tetanus neurotoxin-sensitive and insensitive routes to and from the plasma membrane: fast and slow pathways? Traffic *6*, 366–373.

Proux-Gillardeaux, V., Gavard, J., Irinopoulou, T., Mège, R.-M., and Galli, T. (2005b). Tetanus neurotoxin-mediated cleavage of cellubrevin impairs epithelial cell migration and integrin-dependent cell adhesion. Proc. Natl. Acad. Sci. USA *102*, 6362–6367.

Proux-Gillardeaux, V., Raposo, G., Irinopoulou, T., and Galli, T. (2007). Expression of the Longin domain of TI-VAMP impairs lysosomal secretion and epithelial cell migration. Biol. Cell *99*, 261–271.

Pu, J., Schindler, C., Jia, R., Jarnik, M., Backlund, P., and Bonifacino, J.S. (2015). BORC, a multisubunit complex that regulates lysosome positioning. Dev. Cell *33*, 176–188.

Pu, J., Guardia, C.M., Keren-Kaplan, T., and Bonifacino, J.S. (2016). Mechanisms and functions of lysosome positioning. J. Cell Sci. *129*, 4329–4339.

Rao, S.K., Huynh, C., Proux-Gillardeaux, V., Galli, T., and Andrews, N.W. (2004). Identification of SNAREs involved in synaptotagmin VII-regulated lysosomal exocytosis. J. Biol. Chem. *279*, 20471–20479.

Sander, L.E., Frank, S.P.C., Bolat, S., Blank, U., Galli, T., Bigalke, H., Bischoff, S.C., and Lorentz, A. (2008). Vesicle associated membrane protein (VAMP)-7 and VAMP-8, but not VAMP-2 or VAMP-3, are required for activation-induced degranulation of mature human mast cells. Eur. J. Immunol. *38*, 855–863.

Schäfer, I.B., Hesketh, G.G., Bright, N.A., Gray, S.R., Pryor, P.R., Evans, P.R., Luzio, J.P., and Owen, D.J. (2012). The binding of Varp to VAMP7 traps VAMP7 in a closed, fusogenically inactive conformation. Nat. Struct. Mol. Biol. *19*, 1300–1309.

Sens, P., and Plastino, J. (2015). Membrane tension and cytoskeleton organization in cell motility. J. Phys. Condens Matter *27*, 273103.

Skalski, M., and Coppolino, M.G. (2005). SNARE-mediated trafficking of alpha5beta1 integrin is required for spreading in CHO cells. Biochem. Biophys. Res. Commun. *335*, 1199–1210.

Solon, J., Levental, I., Sengupta, K., Georges, P.C., and Janmey, P.A. (2007). Fibroblast adaptation and stiffness matching to soft elastic substrates. Biophys. J. *93*, 4453–4461.

Steffen, A., Le Dez, G., Poincloux, R., Recchi, C., Nassoy, P., Rottner, K., Galli, T., and Chavrier, P. (2008). MT1-MMP-dependent invasion is regulated by TI-VAMP/VAMP7. Curr. Biol. *18*, 926–931.

Südhof, T.C., and Rothman, J.E. (2009). Membrane fusion: grappling with SNARE and SM proteins. Science *323*, 474–477.

Sun, Z., Guo, S.S., and Fässler, R. (2016). Integrin-mediated mechanotransduction. J. Cell Biol. *215*, 445–456.

Tam, J.H.K., Seah, C., and Pasternak, S.H. (2014). The amyloid precursor protein is rapidly transported from the Golgi apparatus to the lysosome and where it is processed into beta-amyloid. Mol. Brain *7*, 54.

Tayeb, M.A., Skalski, M., Cha, M.C., Kean, M.J., Scaife, M., and Coppolino, M.G. (2005). Inhibition of SNARE-mediated membrane traffic impairs cell migration. Exp. Cell Res. *305*, 63–73.

Toyofuku, T., Morimoto, K., Sasawatari, S., and Kumanogoh, A. (2015). Leucine-rich repeat kinase 1 regulates autophagy through turning on TBC1D2-dependent Rab7 inactivation. Mol. Cell. Biol. *35*, 3044–3058.

Tzvetkova-Chevolleau, T., Stéphanou, A., Fuard, D., Ohayon, J., Schiavone, P., and Tracqui, P. (2008). The motility of normal and cancer cells in response to the combined influence of the substrate rigidity and anisotropic microstructure. Biomaterials *29*, 1541–1551.

Ulbricht, A., Eppler, F.J., Tapia, V.E., van der Ven, P.F.M., Hampe, N., Hersch, N., Vakeel, P., Stadel, D., Haas, A., Saftig, P., et al. (2013). Cellular mechanotransduction relies on tension-induced and chaperone-assisted autophagy. Curr. Biol. *23*, 430–435.

Verderio, C., Cagnoli, C., Bergami, M., Francolini, M., Schenk, U., Colombo, A., Riganti, L., Frassoni, C., Zuccaro, E., Danglot, L., et al. (2012). TI-VAMP/VAMP7 is the SNARE of secretory lysosomes contributing to ATP secretion from astrocytes. Biol. Cell *104*, 213–228.

Williams, K.C., and Coppolino, M.G. (2011). Phosphorylation of membrane type 1-matrix metalloproteinase (MT1-MMP) and its vesicle-associated membrane protein 7 (VAMP7)-dependent trafficking facilitate cell invasion and migration. J. Biol. Chem. *286*, 43405–43416.

Yatsu, A., Shimada, H., Ohbayashi, N., and Fukuda, M. (2015). Rab40C is a novel Varp-binding protein that promotes proteasomal degradation of Varp in melanocytes. Biol. Open *4*, 267–275.

Yudowski, G.A., Puthenveedu, M.A., and von Zastrow, M. (2006). Distinct modes of regulated receptor insertion to the somatodendritic plasma membrane. Nat. Neurosci. *9*, 622–627.

van Zanten, T.S., Cambi, A., Koopman, M., Joosten, B., Figdor, C.G., and Garcia-Parajo, M.F. (2009). Hotspots of GPI-anchored proteins and integrin nanoclusters function as nucleation sites for cell adhesion. Proc. Natl. Acad. Sci. USA *106*, 18557–18562.

Zhang, W., Zong, C.S., Hermanto, U., Lopez-Bergami, P., Ronai, Z., and Wang, L.-H. (2006). RACK1 recruits STAT3 specifically to insulin and insulin-like growth factor 1 receptors for activation, which is important for regulating anchorage-independent growth. Mol. Cell. Biol. *26*, 413–424.

Supplemental Information

Biomechanical Control of Lysosomal

Secretion Via the VAMP7 Hub:

A Tug-of-War between VARP and LRRK1

Guan Wang, Sébastien Nola, Simone Bovio, Philippe Bun, Maïté Coppey-Moisan, Frank Lafont, and Thierry Galli
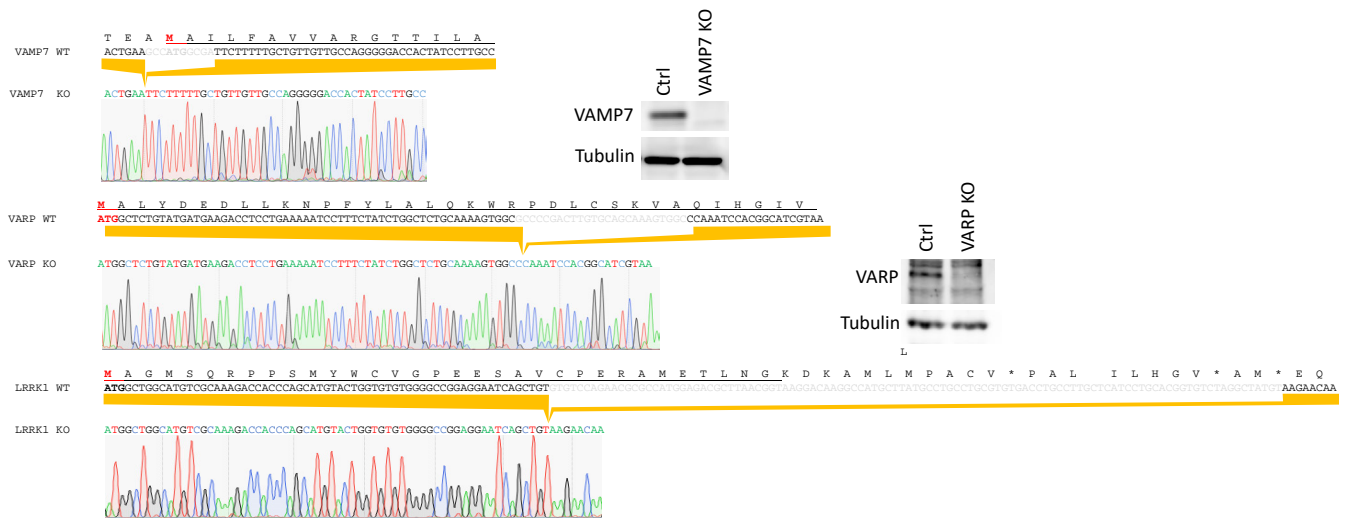
Figure S1. Genotyping and western blot of KO cell lines. Related to Figure 1 and Figure 8.
Left, Genomic DNA sequencing results of the VAMP7, VARP, and LRRK1 CRISPR KO COS7 cell lines. Right, Western blot confirmation of the VAMP7 KO and VARP KO. Two different commercially available antibodies for LRRK1 were tested but were not suitable for western blotting in COS7 cells extract.
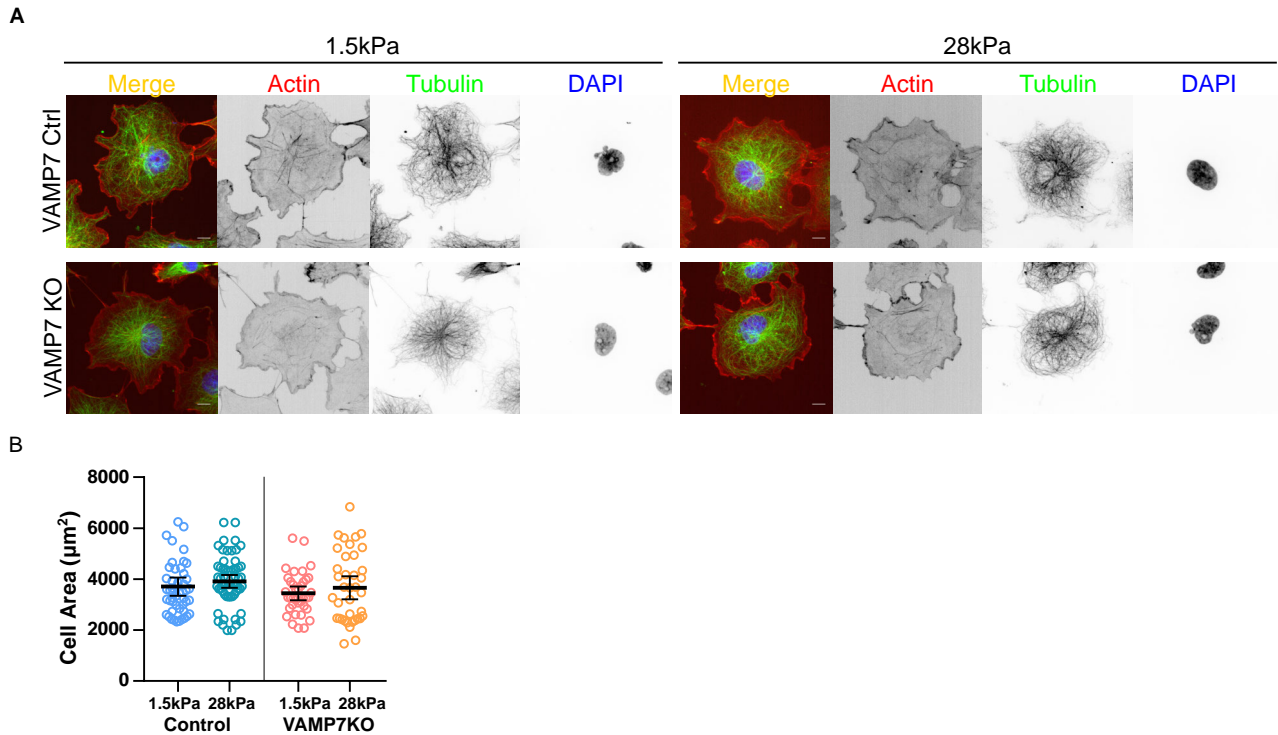
A

1.5kPa   28kPa

Merge | Actin | Tubulin | DAPI   Merge | Actin | Tubulin | DAPI

VAMP7 Ctrl

VAMP7 KO

B

Cell Area (µm²)

1.5kPa 28kPa — Control
1.5kPa 28kPa — VAMP7KO

Figure S2. Cytoskeleton and spreading of COS7 cells grown on PDMS gels. Related to Figure 1.

(A) Representative VAMP7 control or KO COS7 cells grown on laminin coated 1.5kPa or 28kPa PDMS gels for 18-24 hours. Cells were fixed and immunostained with phalloidin and anti-tubulin antibody. Images show z-projection of confocal stack. Scale bar: 10µm.

(B) Quantification of the cell spreading area. No significant difference was found with ANOVA with Tukey's post hoc or Welsh's t-test. Graph shows scatter plot with mean ± 95%CI. n=49, 62, 37, 38 cells respectively.
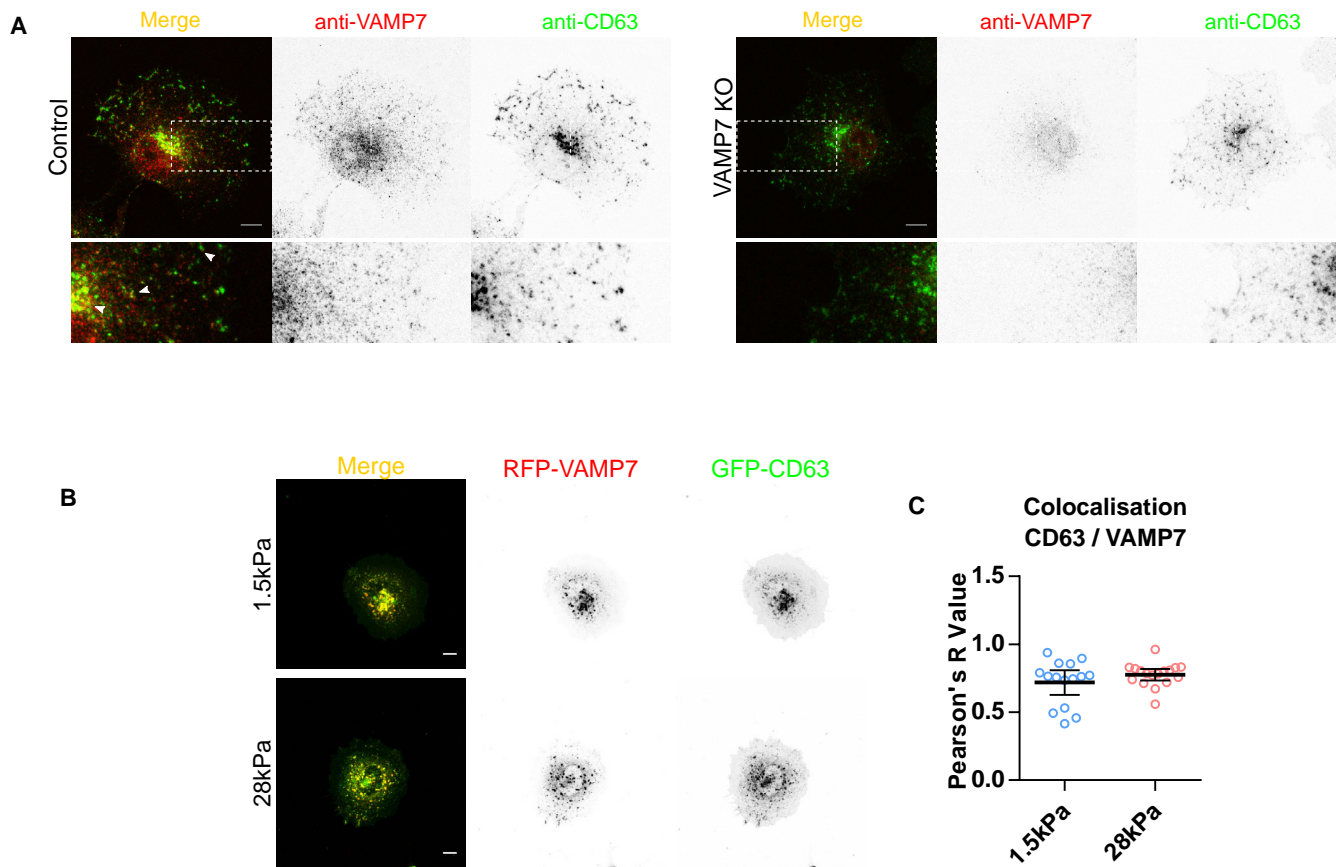
Figure S3. Colocalization between VAMP7 and CD63. Related to Figure 2.

(A) Immunostaining of endogenous VAMP7 and CD63 in COS7 cells grown overnight on laminin coated glass coverslips. Cells were fixed and immunostained for endogenous VAMP7 and CD63. Arrow heads indicates colocalization. Note the low background VAMP7 immunostaining in VAMP7 KO cells. Images show z-projection of confocal stack. For each channel, the same max and min value were set to all the images. Scale bar: 10μm.

(B) Representative COS7 cells expressing RFP-VAMP7 and GFP-CD63 grown on laminin coated1.5kPa and 28kPa PDMS gels for 18-24h. Images show z-projection of confocal stack. Scale bar: 10μm.

(C) Quantification of co-localization. Graph shows scatter plot with mean ± 95% CI. Each point represents the value obtained from a single cell. Data were collected from two independent experiments. 1.5kPa n=11, 28kPa n=16. No significant difference was detected with Mann-Whitney test.
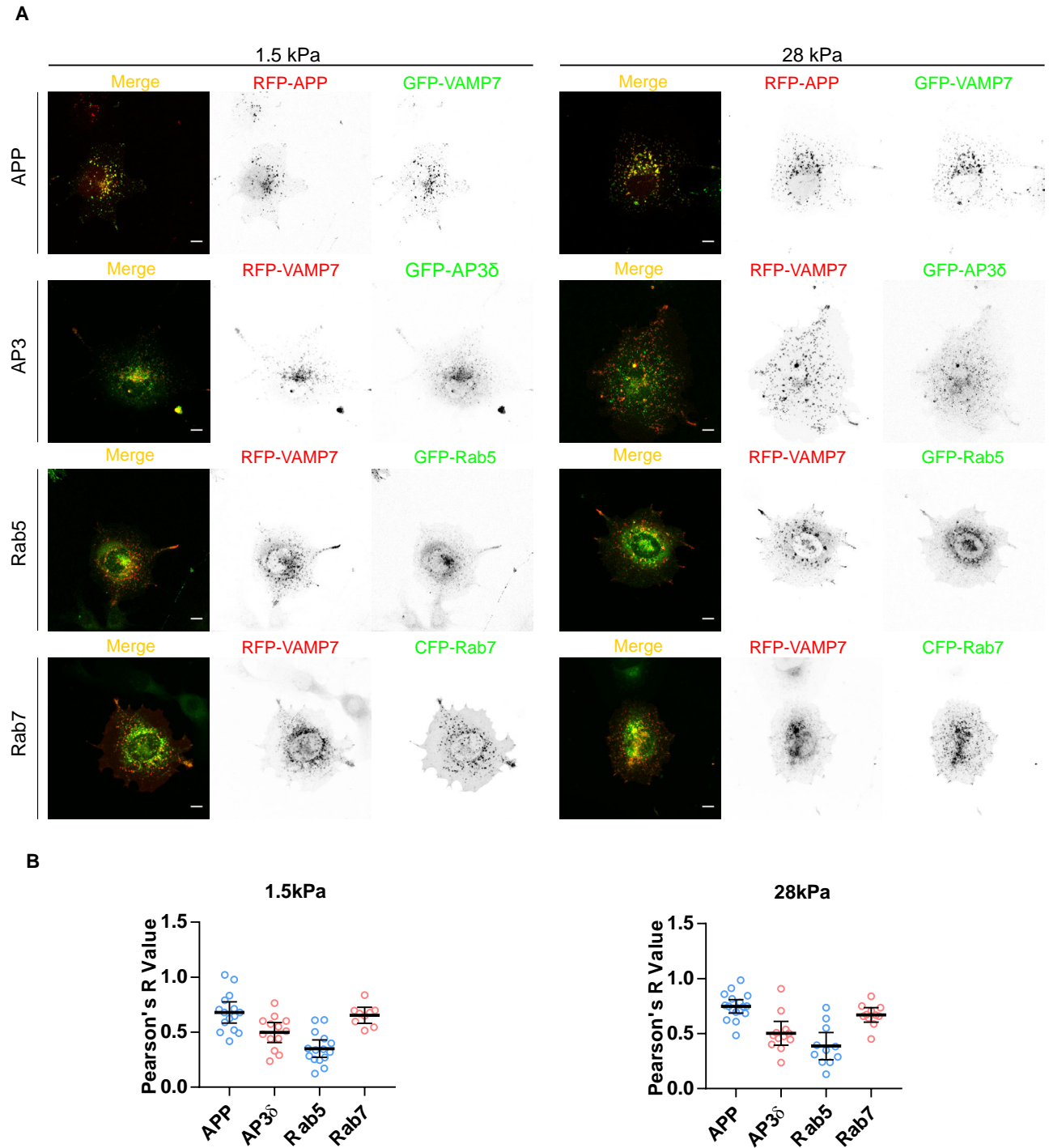
Figure S4. Characterization of the subcellular localization of overexpressed VAMP7. Related to Figure 2.
(A) Representative COS7 cells expressing indicated proteins, grown overnight on laminin-coated glass coverslips. Images show z-projection of confocal stack. Scale bar: 10μm.
(B) Quantification of co-localization. Graph shows scatter plot with mean ± 95% CI. Each point represents the value obtained from a single cell. Data were collected from two independent experiments. 1.5kPa: n=15, 13, 15, 9; 28kPa n=17, 12, 11, 11 respectively.
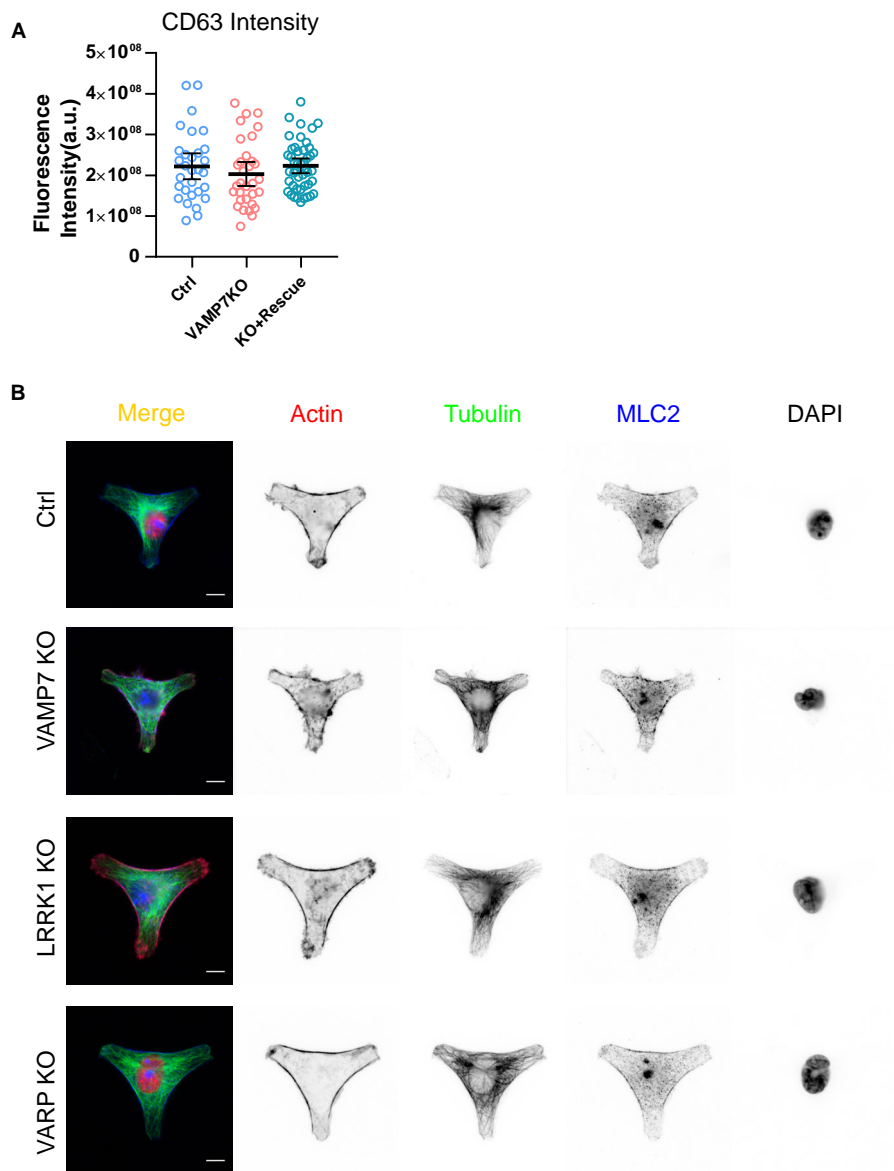
Figure S5. Immunocytochemistry of COS7 cells grown on micropatterns. Related to Figure 2.
(A) Quantification of the endogenous CD63 expressing level by immunocytochemistry in Control, VAMP7 KO and overexpressing cells. No significant difference was found with ANOVA with Tukey's post hoc. Each point represents the integrated intensity of CD63 immunofluorescence. Graph shows scatter plot with mean ± 95%CI. n=30, 32, 46 cells respectively.
(B) Representative Control, VAMP7 KO, LRRK1 KO and VARP KO COS7 cells grown on laminin Y patterns for 4 hours. Cells were fixed and immunostained for actin, tubulin and myosin light chain2 (MLC2). Images show z-projection of confocal stack. Scale bar: 10μm.
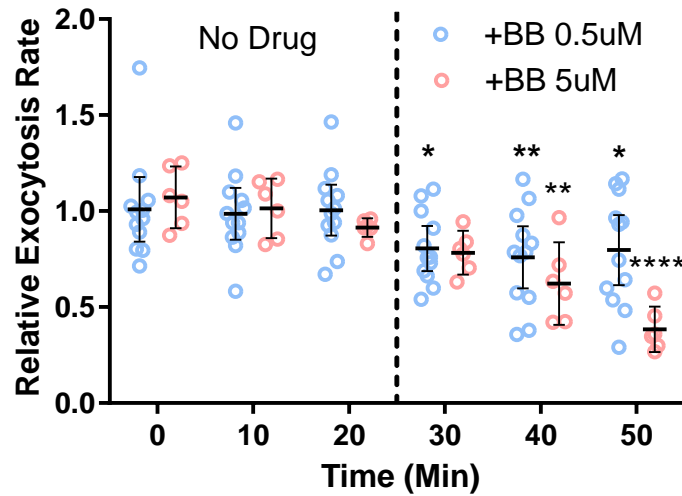
Figure S6. Blebbistatin inhibits VAMP7 exocytosis. Related to Figure 3.
Relative frequency of vesicle fusion in COS7 expressing VAMP7-pHluorin plated on laminin coated glass coverslip. Time-lapse videos were acquired during 1min for each cell every 10min. Blebbistatin was added to a final concentration of 0.5μM or 5μM after the third time point. Exocytosis frequency was normalized to the 1st acquisition (t=0min). Graph shows scatter plot with mean ± 95% CI. Data presented is pooled from 2 independent experiments. BB 0.5μM: n = 12, BB 5μM: n = 6. Value at t=30, t=40 and t=50 were compared to the average value of no drug condition. *$p<0.05$, **$p<0.01$, ****$p<0.0001$. Significance is determined by Two-way ANOVA with Dunnett's post-hoc test.

Figure S7. Quantification of the half-life of VAMP7-pHluorin signals. Relate to Figure 3 and Figure 4.

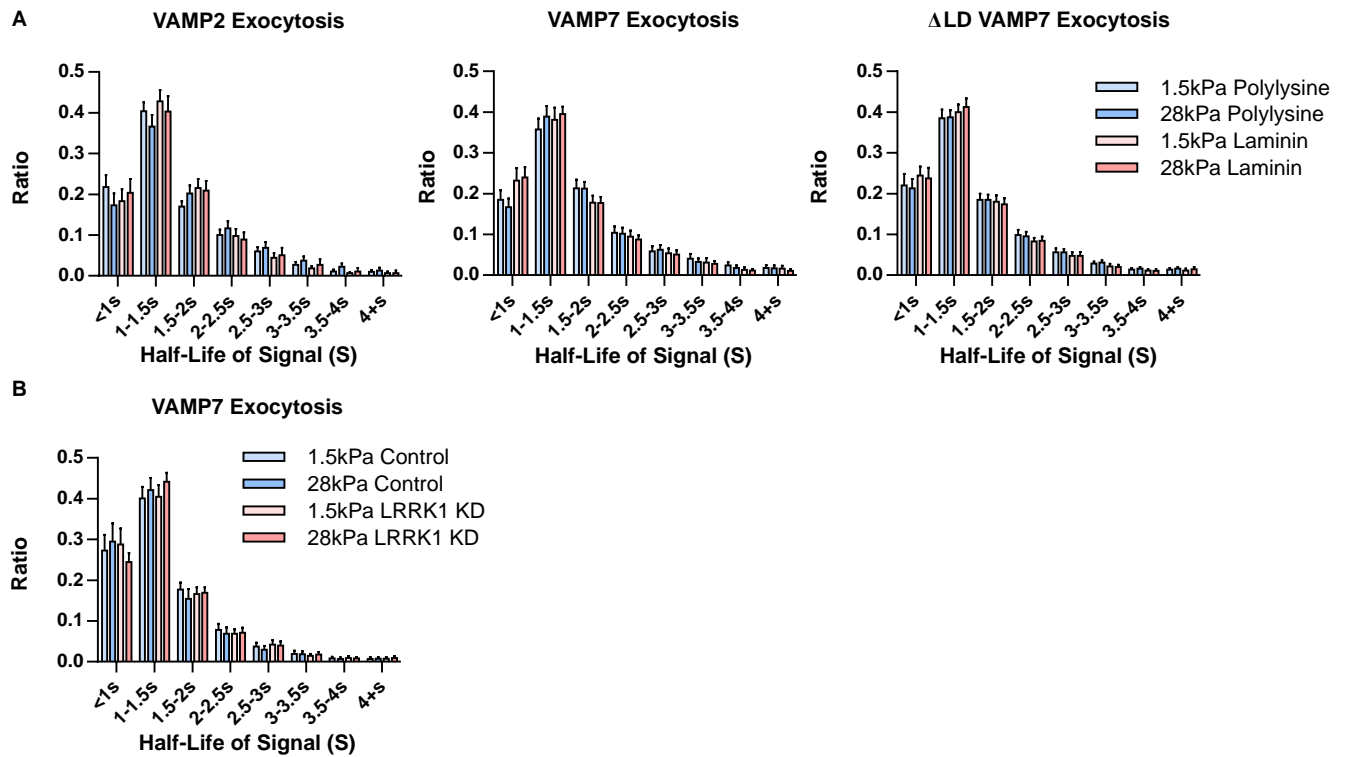Quantification of the half-life of VAMP7-pHluorin signals, which represent the kinetics of fusion, pore opening and spreading followed by endocytosis and re-acidification. Frequency distribution of different temporal classes of exocytic events are indicated on the abscissa. Bar graph shows mean with 95% CI.
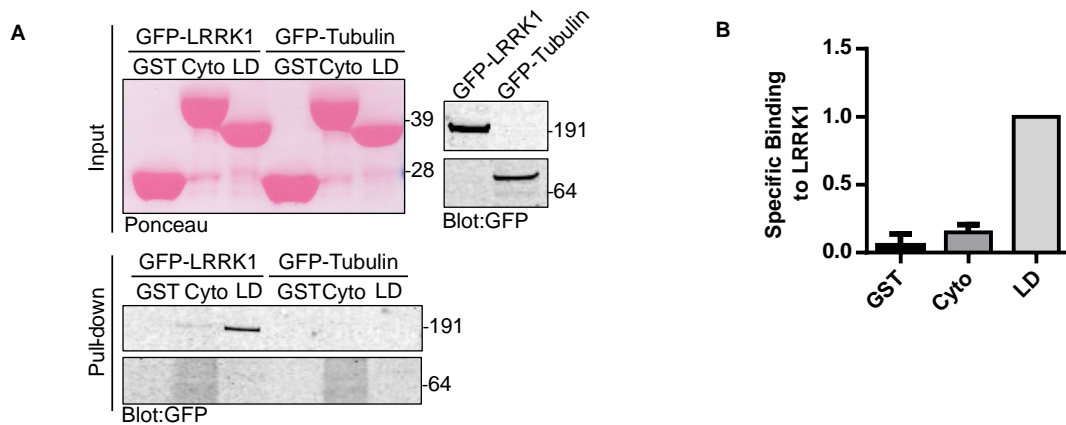
Figure S8. In vitro binding assay between GST-tagged VAMP7 domain and LRRK1. Related to Figure 5.

(A) Lysates from COS7 cells expressing GFP-LRRK1 or GFP-Tubulin were incubated with purified control GST, GST-tagged cytosolic domain (Cyto), and Longin (LD) of VAMP7 protein. Ponceau S stain showing the relative amount of the different GST-tagged proteins coupled to the glutathione beads at the end of the experiment and control GFP immunoblot. Precipitated proteins were subjected to SDS-PAGE, and the blots were stained with antibodies against GFP. Experiments were repeated twice with similar results.

(B) Quantification of the binding assays. Precipitated GFP-Tubulin signal, defined as background, was subtracted to precipitated GFP-LRRK1 signal in each pull down condition (GST, Cyto, LD). GFP-LRRK1 pulled down by LD was arbitrarily set to 1 in each experiment. n = 2 independent experiments. Graph shows mean ± SD.
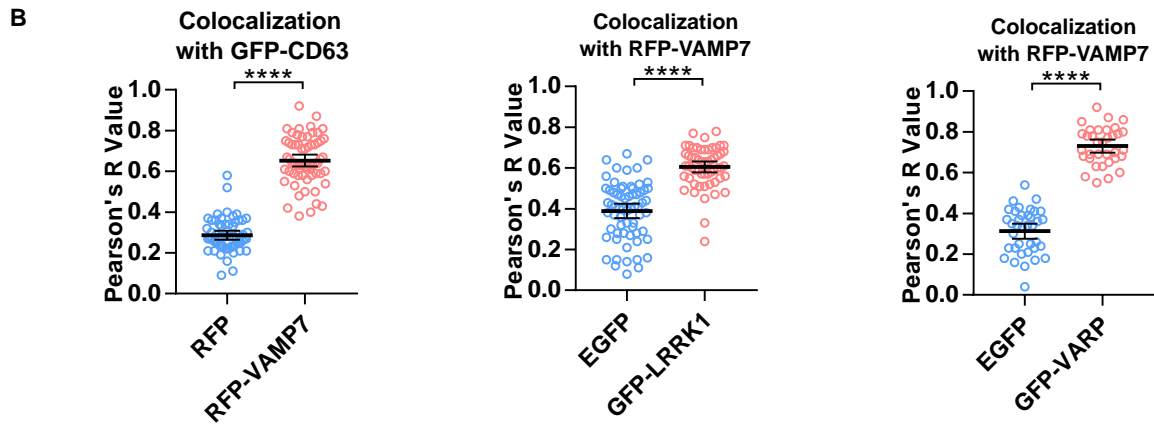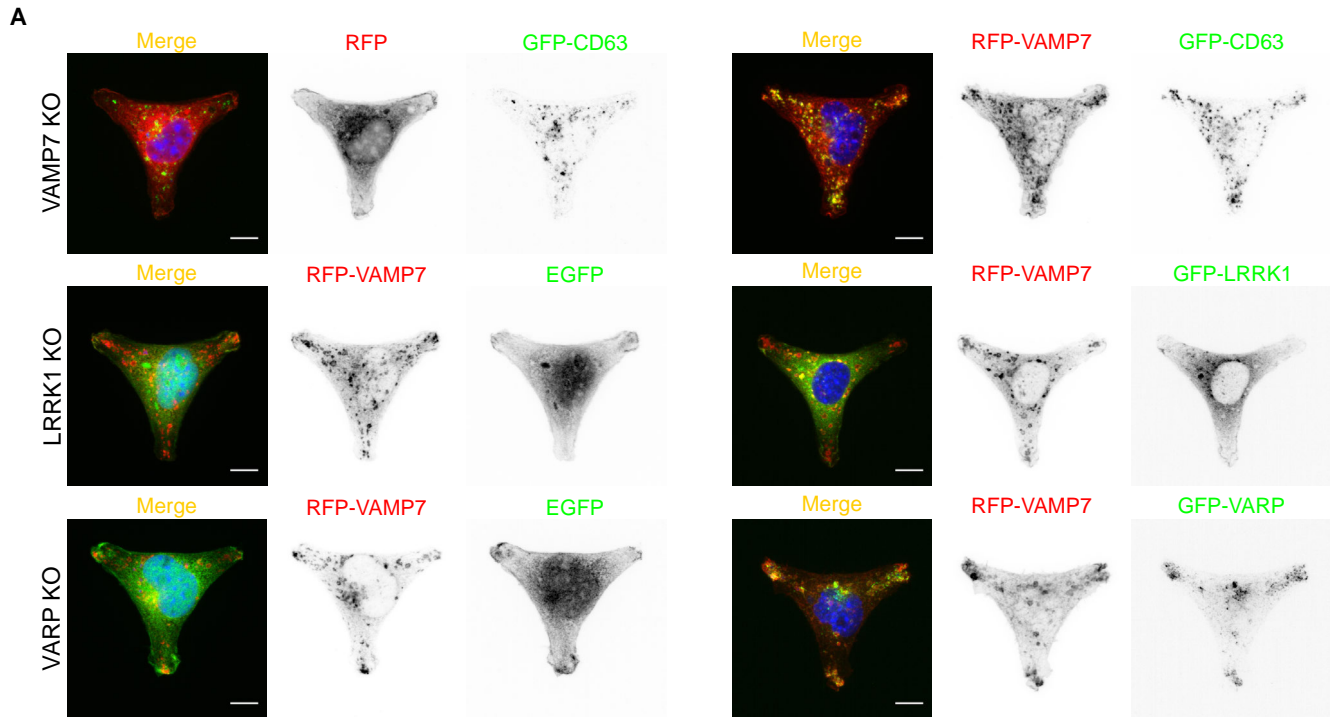
Figure S9. Colocalization assay in rescued KO cells. Related to Figure 5 and Figure 8.
(A) Representative COS7 VAMP7 KO cells re-expressing RFP-VAMP7 or RFP and GFP-CD63, LRRK1 KO cells re-expressing GFP-LRRK1 or GFP and RFP-VAMP7, VARP KO cells re-expressing GFP-VARP or GFP and RFP-VAMP7, grown on laminin-coated Y patterns for 4 hours. Images show z-projection of confocal stack. Scale bar: 10μm.
(B) Quantification of co-localization. Graph shows scatter plot with mean ± 95% CI. Each point represents the value obtained from a single cell. Data were collected from two independent experiments. VAMP7 KO: RFP n=59, RFP-VAMP7, n=63; VARP KO: EGFP n=65, GFP-LRRK1 n=56; LRRK1 KO: EGFP n=37, GFP-VARP n=34. ****p<0.0001, Welch's t test was used.

A

GAPDH

LC3-I
LC3-II

1.5kPa 28kPa 1.5kPa 28kPa
Polylysine **Laminin**

B

1.5kPa 28kPa 1.5kPa 28kPa
Poly-lysine **Laminin**
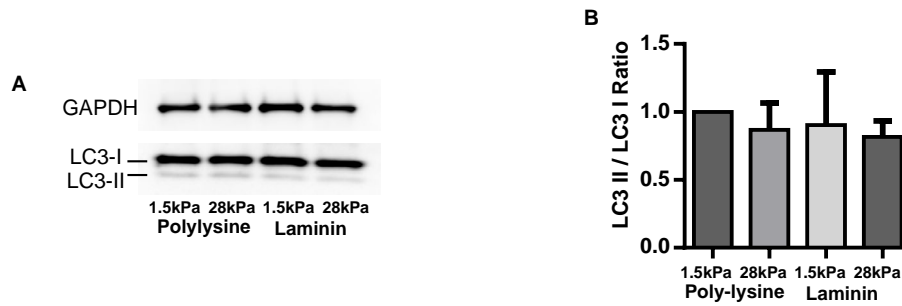
Figure S10. Substrate rigidity does not trigger autophagy in COS7 cells. Related to Figure 6.
(A) Immunoblot analysis of LC3 and GAPDH in extracts of COS7 cells grown on polylysine- or
laminin-coated PDMS gel of 1.5kPa or 28kPa for 18-24 hours. Experiments were independently
repeated three times with similar result.
(B) Quantification of the LC3-II signals over the LC3-I signals. Signals were normalized to the
1.5kPa polylysine condition in each manipulation. Bar graph shows mean ± SD, n=3. No
significant difference was found with ANOVA with Tukey's post hoc or Welsh's t-test.
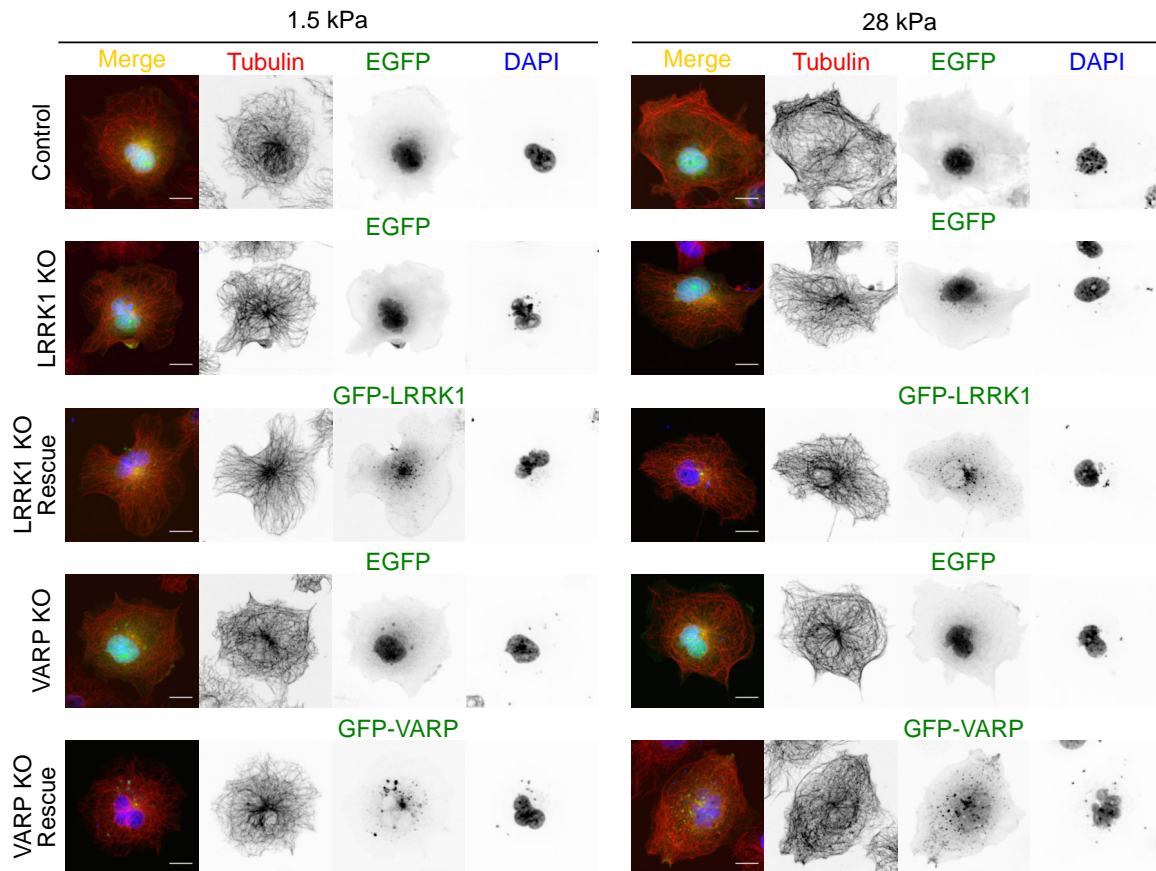
Figure S11. Microtubules of KO cells and recued cells. Related to Figure 8.
Representative Control, LRRK1 KO and VARP KO COS7 cells grown on laminin-coated PDMS gels. Control and KO cells were transfected with EGFP or GFP-LRRK1 or GFP-VARP as indicated. Cells were fixed and immunostained for tubulin. Images show z-projection of confocal stack. Scale bar: 10μm.

Table S1. Quantification of the binding assays in Figure 5C. Related to Figure 5.

| Sample	Mean	SD	SEM	n	P value (t-test, two tailed)
1-220	1	n/a	n/a	3	n/a
1-98	0.9038	0.3974	0.2294	3	ns, 0.7156
1-120	0.5976	0.2295	0.1325	3	*, 0.0935
99-120	0.08472	0.01813	0.01047	3	***, 0.0001
102-220	1.005	0.3093	0.1786	3	ns, 0.9815
121-220	0.4814	0.1557	0.08987	3	*, 0.0287
G4SX4	1.085	0.4994	0.2884	3	ns.0.7969
mRFP	0.04984	0.019	0.01097	3	***, 0.0001
1-220	0.07008	0.05006	0.0289	3	**, 0.001
G4SX4	0.01588	0.00576	0.003325	3	****, <0.0001
The RFP-VAMP7 IP signals ware normalized to the GFP-LRRK1 IP signals for each lane. The ratio of VAMP7 1-220 was arbitrarily set to 1.					

Table S2. Quantification of the binding assays in Figure 5 D. Related to Figure 5.

Sample	Mean	SD	SEM	n	P value (t-test, two tailed)
1-220	1	n/a	n/a	3	n/a
1-98	0.2397	0.07918	0.04572	3	*, 0.0036
1-120	0.07519	0.03102	0.01791	3	***, 0.0004
99-120	0.03609	0.02732	0.01577	3	***, 0.0003
102-220	1.06	0.9086	0.5246	3	ns, 0.9195
121-220	0.1989	0.08302	0.04793	3	*, 0.0036
G4SX4	0.8711	0.4006	0.2313	3	ns* 0.6335
mRFP	0.02173	0.01652	0.009537	3	****, <0.0001
1-220	0.04619	0.0071	0.004099	3	****, <0.0001
G4SX4	0.008139	0.000829	0.000479	3	****, <0.0001
The RFP-VAMP7 IP signals ware normalized to the GFP-VARP IP signals for each lane. The ratio of VAMP7 1-220 was arbitrarily set to 1.					

Table S3. Quantification of the binding assays in Figure 5 E. Related to Figure 5.

Sample	Mean	SD	SEM	n	P value (t-test, two tailed)
myc	1	n/a	n/a	3	n/a
myc-ID-FLAG	0.6374	0.1434	0.0828	3	*, 0.0484
Co-precipitated RFP signal was normalized to the trapped GFP signal for each condition. Control condition, corresponding to the expression of the myc vector without ID-FLAG insert, was arbitrarily set to 1 for RFP-VAMP7 co-precipitated with GFP-LRRK1.					

Table S4. Quantification of the binding assays in Figure 5 F. Related to Figure 5.

Sample	Mean	SD	SEM	n	P value (t-test, two tailed)
myc	1	n/a	n/a	3	n/a
myc-ID-FLAG	0.5331	0.1202	0.06941	3	*, 0.0214
Co-precipitated RFP signal was normalized to the trapped GFP signal for each condition. Control condition, corresponding to the expression of the myc vector without ID-FLAG insert, was arbitrarily set to 1 for RFP-VAMP7 co-precipitated with GFP-VARP.					

Table S5. Quantification of the binding assays in Figure 7 C. Related to Figure 7.

Sample	Mean	SD	SEM	n	P value (t-test, two tailed)
WT	1	n/a	n/a	3	n/a
Y944F	1.319	0.3511	0.2027	3	ns, 0.2561
K1243M	0.8513	0.449	0.2592	3	ns, 0.6242
The RFP IP signals were normalized to the GFP IP signals for each lane. The ratio of LRRK1 WT was arbitrarily set to 1					

Transparent Methods

Atomic force microscopy

COS7 cells were plated on PDMS substrates 24 hours before the experiment. Experiments were performed at 37°C on a commercial stand-alone AFM (NanoWizard3, JPK Instruments) combined with an inverted optical microscope (AxioObserver.Z1, Zeiss) driven by JPK NanoWizard software 6.0 and Zen Blue 2012. AFM was operated in Quantitative Imaging (QI) mode in serum-free culture medium (DMEM), supplemented with 20 mM Hepes, using PFQNM-LC probes with a nominal spring constant of 0.033 N/m and radius of curvature R of 65 nm. One single tip has been used for all the experiments. The thermal tune method was used before each experiment to correct the deflection sensitivity value in order to obtain reproducible spring constant measurements, as established by the Standardized Nanomechanical Atomic Force Microscopy Procedure protocol SNAP (Schillers et al., 2017), which guarantees a reproducible calibration, an essential step for obtaining robust and comparable results between different experiments.

Using QI mode we performed 16x16 pixel force mapping scans over 20μm x 20μm areas. We applied a force trigger of 0.5 nN with a 2.5 μm z ramp, at 70 μm/s speed. Similar areas located on the periphery of the cell, including a part of substrate, were chosen. Force curves were processed using in-house developed software pyAF. Elasticity was calculated as Young's modulus over the first 75 nm of indentation, using the Hertz model (that describes the contact mechanics between a hard sphere and perfectly elastic homogeneous and isotropic half-space) corrected to account for the finite height of the cell (Dimitriadis et al., 2002), as follows:

$$F = \frac{4}{3}\frac{E}{(1-\nu^2)} R^{1/2}\delta^{3/2}[1 + 1.133X + 1.283X^2 + 0.769X^3 + 0.0975X^4]$$

F: Force, E: Young's modulus, R: Tip radius, δ: indentation, ν: Poisson's ratio (conventionally set to 0.5 for cells), X: δ/h with h: sample thickness.

Four independent experiments have been performed per cell types.

Antibodies

The following antibodies were used in this study: Mouse anti-CD63 antibody from Abcam (ab193349); Mouse anti-GFP antibody from Roche (11814460001); Goat anti-mCherry antibody from Acris (AP32117PU-S); Mouse anti-FLAG antibody from Covalab (mab90006-P); Rabbit anti-LRRK1 antibody from Sigma (HPA010537) and from Abgent (Ap7098b); Rabbit anti-MLC2 was from Cell Signaling (#3672); Goat anti-mouse Alexa Fluor 488- and

633-conjugated secondary antibody from ThermoFisher. Donkey anti-mouse and donkey anti-rabbit HRP-conjugated secondary antibody from Jackson ImmunoResearch. Rabbit polyclonal antibody against interaction domain of VAMP7 in VARP (ID, amino acids 641 to 709) (pAb TG40) and polyclonal (TG18) and monoclonal (Clone 158.2) antibodies against VAMP7 were produced in the lab and described previously (Burgo et al., 2009; Galli et al., 1998; Muzerelle et al., 2003).

cDNAs

pHluorin-tagged VAMP2 was a kind gift from Dr. Tim Ryan (Cornell University, USA). pHluorin-tagged forms of WT VAMP7 [1-220] and Δ[1-125] mutant were previously described (Burgo et al., 2012, 2013). VAMP7 fragments used in binding assay were cloned by PCR and inserted into pmRFP-C1 vector between SalI and BamHI site. To make VAMP7 G4S mutant, VAMP7 [1-100], VAMP7[121-220] and [GGGGS]x4 were ligated into pmRFP-C1 vector between SalI and BamHI site using Gibson assembly (NEB). The [GGGGS]x4 sequence was:

GGTGGAGGAGGTTCAGGAGGAGGTGGATCTGGAGGTGGCGGATCGGGTGGTGGA GGTTCT. GFP-Varp and GFP-Tubulin were previously described (Burgo et al., 2009, 2012; Martinez-Arca et al., 2003). GFP-tagged LRRK1 WT, Y944F, and K1243M mutants were generous gift from Dr. Hiroshi Hanafusa (Nagoya University, Japan). LRRK1 shRNA plasmid (sc-149115-SH) and control shRNA plasmid (sc-108060) were purchased from Santa Cruz. VARP-flag construct was cloned in pcDNA3.1 by the molecular biology facility BM-GIF/Imagif (Gif-sur-Yvette, France). Briefly, a 3xGGS linker sequence followed by flag tag was added carboxy-terminally to human VARP sequence using GeneArt Seamless Cloning and Assembly kit (Invitrogen). A mutant of VARP unable to bind VAMP7 (Schäfer et al., 2012) was generated by site-directed mutagenesis of aa D679 and D681 into A thus generating the so-called DADA mutant. The interaction domain of VAMP7 in VARP (ID, aa 641 to 709) (Burgo et al., 2009, 2012) was subcloned in pcDNA3.1, flanked by amino-terminal Myc and carboxy-terminal FLAG tags.

Cell Culture, Cell Transfection, and Substrate

COS7 cells were cultured in DMEM with 1g/L supplied with 10% FBS (Gibco) in a 5% CO2-humidified atmosphere at 37 °C. For pHluorin video imaging, COS7 cells were transfected by using Lipofectamine 2000 (Life Technologies). For the other experiments, COS7 cells were transfected by using X-tremeGENE HP (Roche) following the manufacturer's instructions. Sucrose (84097) and EGF (E41247) used in the perfusion mediums were purchased from Sigma. Glass bottom imaging dishes were purchased from ibidi (81218). Imaging dishes with a PDMS Elastically Supported Surface (ESS 1.5kPa and 28kPa) were purchased from ibidi

(81291, 81191). The surface of PDMS is activated for 1 min in a plasma cleaner (Aldrich Z561665) before coating. Polyacrylamide gels were made following published protocol (Tse and Engler, 2010). Micropatterned imaging chips (Pattern size: Large; Cell area: 1600μm²; Micropattern line width: 8 μm) were purchased from CYTOO (10-900-00, 10-012-00). Substrates were coated overnight with 100μg/ml polylysine (P2636, Sigma) in borate buffer pH8.0 then 10μg/ml laminin (L2020, Sigma) in DPBS.

Direct and indirect fluorescence sample preparation

COS7 cells were co-transfected on 35-mm culture dishes using XtremeGene as described below. After 24 h, these cells were split on laminin-coated substrates at a density of $1x10^4$ cells/cm². 18-24h after plating, the cells were fixed with 4% for 20min at room temperature, mounted in Mowiol-DABCO anti-fading medium and dried overnight at room temperature. For immunostaining, cells were permeabilized with 0.1% triton for 4min after fixation, incubated with primary antibodies o/n at 4 degrees, and secondary antibodies for 1h at room temperature. with DAPI for 10min in the second wash. Specimens were stored at 4°C until imaging.

EGF stimulation assay

COS7 cells were co-transfected on 35-mm culture dishes with 0.5μg RFP- tagged VAMP7 or VAMP7 ΔLD mutant, and with 0.5μg GFP-tagged LRRK1 by using XtremeGENE HP. After 24 h, These cells were split on polylysine- or laminin-coated PDMS gels at a density of 1x104 cells/cm2. Time-lapse videos were recorded at 1min intervals using the same wild-field microscopy as described in pHluorin imaging assay with a 1.6X mag changer and a 63X/1.4 NA Plan-Apochromat oil immersion Leica objective. EGF were injected into imaging chamber between time point -1min and 0min at a final concentration of 100ng/ml. The relative fluorescence intensity was measured inside a 16μm diameter oval around the cell center (materialized as a dashed circle in Figure 6 B) and compared to the total fluorescence intensity. The result was then normalized to the ratio before adding EGF.

Generation of depleted cell lines

To produce COS7 CRISPR knockout cell lines for VAMP7, VARP and LRRK1, we generated RNA-CAS9 guide constructs based on published protocol (Ran et al., 2013). Briefly, oligonucleotides targeting sequences near the translation starting site of the gene of interest were designed using the "RGEN Cas designer" web-based tool (Park et al., 2015) that encompasses *Chlorocebus sabeus* sequence database. To limit off-targets, sequence of oligo with ≤ 2 putative mismatches throughout the whole genome or an 'out of frame' score <66 were excluded. The primer sequences are:

For VAMP7, forward primer: 5'- caccgAACAGCAAAAAGAATCGCCA-3', reverse primer: 5'- aaacTGGCGATTCTTTTTGCTGTTc-3';

For VARP, forward primer: 5'-caccgCCCCGACTTGTGCAGCAAAG-3', reverse primer: 5'-aaacCTTTGCTGCACAAGTCGGGGc-3' ;

For LRRK1, forward primer: 5'-caccgTGTGTGTCCAGAACGCGCCA-3', reverse primer: 5'-aaacTGGCGCGTTCTGGACACACAc-3'.

Each pair of oligonucleotides (10mM) was heated at 95°C for 5 min and annealed by ramping down the temperature from 95°C to 25°C at 5°C min-1. Annealed oligonucleotides were ligated into pSpCas9(BB)-2A-Puro (PX459) vector (Addgene) using the BbsI sites. After validation by sequencing, the targeting constructs were transfected into COS7 cells. At 24h post-transfection, cells were diluted and transfected cells were selected by 3μg/ml puromycin addition. Selected population were then seeded into a 96-well plate at <1 cell per well. Clones derived from single cells were obtained and screened for deficiency by genomic PCR and sequencing, and immunoblotting (except for LRRK1 due to low endogenous level of expression in COS7 cells and/or poor reactivity of available antibodies against monkey protein).

Immunoprecipitation

COS7 cells were co-transfected in 25cm2 culture flasks with RFP-VAMP7 or mRFP as control, and 1.5μg GFP-LRRK1, GFP-VARP or EGFP as control by using XtremeGENE HP. Cells were transferred into a 10cm petri culture dish 24h after transfection. Cells were then lysed 24h after in a buffer containing 50mM Tris-HCl, pH8.0, 150mM NaCl, 2mM EDTA, 1% NP-40 and Complete tablet (Roche Diagnostics). 1 mg of protein extract and submitted to immunoprecipitation overnight at 4 °C with 20μl GFP-nanotrap sepharose beads produced as described (Rothbauer et al., 2008) under head-to-head agitation. After six washes with lysis buffer, bound proteins were eluted at 95°C for 5min in LDS sample buffer (Life technologies). Eluted proteins were processed for SDS-PAGE and western blot by using Novex 4–20% Tris-Glycine gradient gels (Life technologies) or RunBlue SDS Protein Gels 4-20% (Expedeon), and nitrocellulose membranes (GE). The membranes were blocked with 5% milk in TBST, cut and blotted with anti-GFP and anti-mCherry antibodies. After washing, the membranes were blotted with HRP-tagged secondary antibodies. Revelation was carried out by using a Fujifilm LAS4000 luminescence imager.

Intensity Profile

Cell center was defined as the centroid of the cell using ImageJ script. The background is subtracted and then the intensity profiles were got using Radial Profile Plot plugin (https://imagej.nih.gov/ij/plugins/radial-profile.html) in ImageJ.

In Vitro GST pull-down Assays

The GST-tagged VAMP7 cytoplasmic domain, VAMP7 Longin domain proteins and GST alone were produced as previously described (Martinez-Arca et al., 2000). COS7 cells were transfected in 25cm2 culture flasks with 3μg GFP-LRRK1 WT, GFP-LRRK1 mutants and GFP-Tubulin as a control by using XtremeGENE HP. Cells were lysed 48 h after transfection in a buffer containing 50mM Tris-HCl, pH 8.0, 150mM NaCl, 1mM EDTA, 1% NP40 and Complete tablet (Roche). Lysates were transferred to a 96-well microplate, and fluorescence of GFP was measured at 488 nm using a Fluorescence Plate Reader (Wallac 1420 Victor2 Microplate Reader, PerkinElmer Life Sciences). Lysates were diluted with cell lysate from non-transfected cell to obtain an equal fluorescence intensity. 10μl Glutathione beads were added to 1ml lysates and were incubated overnight with 50μg purified GST-VAMP7 fragments or GST alone as a control. After five washes with lysis buffer, bound proteins were eluted at 70°C for 10min in LDS sample buffer (Life technologies). Eluted proteins were processed for SDS-PAGE and western blot as described above.

Microscopy and image analysis

Time-lapse videos were recorded using a Leica DMI6000B inverted microscope with a 1.6X mag changer, a Leica 63X/1.4 NA Plan-Apochromat oil immersion objective, a 488-Ar ion laser, a iLas2 targeted-laser illumination controller and a Photometrics Cascade II 512 EMCCD camera.

Z-stacks were acquired using an Zeiss LSM 780 confocal microscopy with a Zeiss Plan-Apochromat 63X/1.40 NA oil-immersion objective,or a CSU-W1 (Yokogawa–Andor) spinning disk confocal module installed on a Leica DMI8 microscope with a sCMOS Orca-Flash 4 V2+ camera (Hamamatsu), with a Leica Plan-Apochromat 63X or 100X 1.40 NA oil-immersion objective.

Live cell imaging experiments (pHluorin and Osmotic shock movies, EGF stimulation assay) were carried out with the Leica DMI6000B videomicroscope. Z-stacks for experiments with micropatterns (Fig. 2 A and C, Fig. S5 B, Fig. S9 A) and KO cells (Fig. 8 C) were acquired with the CSU-W1 system with 100X and 63X objective respectively. All the other images were acquired with the Zeiss LSM 780 microscope.

Images were proceeded and analyzed using ImageJ software. Z-projections were made with SUM option, and the contrast of images was adjusted by using "Enhance Contrast" command. Cell spreading area was measured in ImageJ with using the actin channel.

Osmotic shocks

COS7 cells were transfected and plated on laminin-coated 28kPa PDMS gels as mentioned above. Imaging dishes were closed with a homemade lid possessing two luer connectors connected to a peristaltic pump. 2X osmolarity imaging buffer was prepared by adding 300mM sucrose in live cell imaging buffer. Osmotic shocks were performed by perfusing the 2X buffer into imaging dish for 5min and then washed out by normal buffer. The volume of buffer in the chamber was ~0.5ml and was perfused at a rate of 1.5-2 ml/min. Time-lapse videos were recorded at 0.5s intervals by using a Leica DMI6000B inverted microscope as described above.

pHluorin imaging and analysis

COS7 cells were transfected on 35-mm culture dishes with 1μg pHluorin-tagged VAMP2, VAMP7 or ΔLD-VAMP7 plasmids by using lipofectamin2000. For LRRK1 knockdown assays, COS7 cells were co-transfected with 1μg VAMP7 plasmid and 1μg LRRK1 shRNA plasmid or control shRNA plasmid by using lipofectamine2000. The transfection mixture was replaced with new culture medium 3 hours later. After 24 h, These cells were split on polylysine- or laminin-coated PDMS gels at a density of $1x10^4$ cells/cm^2. 18-24h after plating, the cells were processed to live cell imaging.

Time-lapse videos were recorded at 0.5s intervals for 2min by using a Leica DMI6000B inverted microscope as described above. Cells were imaged in live cell imaging buffer (140 mM NaCl, 2.5 mM KCl, 1.8 mM CaCl$_2$, 1.0 mM MgCl$_2$, 20 mM HEPES, 4.5g/ml glucose, and pH=7.4) and kept at 37°C. Cells that had visible exocytosis (>1 event per 6 seconds) were randomly selected.

For blebbistatin inhibition assays, time-lapse videos were recorded at 0.5s intervals for 1min on a same cell every 10min. Blebbistatin was added to a final concentration of 0.5μM or 5μM after the third time point.

Exocytic events of pHluorin were detected using custom-written scripts in ImageJ and Matlab software as described previously (Burgo et al., 2013). Briefly, time-lapse stacks were processed to reveal all sudden appearance of fluorescent spots. Average intensity of fluorescence was measured in a 5 x 5-pixel region of interest centered on each interested spot for each slice. Fluorescent traces were then analyzed, filtered and fitted. Events were defined

as a transient increase of fluorescence followed by an exponential decay. Half-life of events was calculated from the decay curve.

Quantification of perinuclear fluorescence

The perinuclear area in Fig. 8 was defined as the area within 5μm of the nucleus. The nucleus area was defined by DAPI signal. Then the area was enlarged by using" Dilate" function in ImageJ. The cell center in Fig.7 A and B was defined as the local mass center using an ImageJ script. Firstly, the maximum fluorescent point (maxima) close to the nucleus was found. Then the mass center of area inside a 16 μm diameter oval around the maxima was calculated and defined as the local mass center. The fluorescence intensity of RFP-VAMP7 was measured in a 10μm diameter oval and then reported to its total intensity in the cell.

Statistical analysis

GraphPad Prism software were used for statistical analyses. Data were analyzed using Welsh's t-test or one-way ANOVA followed by a Tukey post hoc test as indicated in legends.

Bibliography

1. Schillers H, Rianna C, Schäpe J, Luque T, Doschke H, Wälte M, et al. Standardized nanomechanical atomic force microscopy procedure (SNAP) for measuring soft and biological samples. Sci Rep. 2017 Jul 11;7(1):5117.

2. Dimitriadis EK, Horkay F, Maresca J, Kachar B, Chadwick RS. Determination of elastic moduli of thin layers of soft material using the atomic force microscope. Biophys J. 2002 May;82(5):2798–810.

3. Muzerelle A, Alberts P, Martinez-Arca S, Jeannequin O, Lafaye P, Mazié JC, et al. Tetanus neurotoxin-insensitive vesicle-associated membrane protein localizes to a presynaptic membrane compartment in selected terminal subsets of the rat brain. Neuroscience. 2003;122(1):59–75.

4. Burgo A, Sotirakis E, Simmler M-C, Verraes A, Chamot C, Simpson JC, et al. Role of Varp, a Rab21 exchange factor and TI-VAMP/VAMP7 partner, in neurite growth. EMBO Rep. 2009 Oct;10(10):1117–24.

5. Galli T, Zahraoui A, Vaidyanathan VV, Raposo G, Tian JM, Karin M, et al. A novel tetanus neurotoxin-insensitive vesicle-associated membrane protein in SNARE complexes of the apical plasma membrane of epithelial cells. Mol Biol Cell. 1998 Jun;9(6):1437–48.

6. Burgo A, Proux-Gillardeaux V, Sotirakis E, Bun P, Casano A, Verraes A, et al. A molecular network for the transport of the TI-VAMP/VAMP7 vesicles from cell center to periphery. Dev Cell. 2012 Jul 17;23(1):166–80.

7. Burgo A, Casano AM, Kuster A, Arold ST, Wang G, Nola S, et al. Increased activity of the vesicular soluble N-ethylmaleimide-sensitive factor attachment protein receptor TI-VAMP/VAMP7 by tyrosine phosphorylation in the Longin domain. J Biol Chem. 2013 Apr 26;288(17):11960–72.

8. Martinez-Arca S, Rudge R, Vacca M, Raposo G, Camonis J, Proux-Gillardeaux V, et al. A dual mechanism controlling the localization and function of exocytic v-SNAREs. Proc Natl Acad Sci U S A. 2003 Jul 22;100(15):9011–6.

9. Schäfer IB, Hesketh GG, Bright NA, Gray SR, Pryor PR, Evans PR, et al. The binding of Varp to VAMP7 traps VAMP7 in a closed, fusogenically inactive conformation. Nat Struct Mol Biol. 2012 Dec;19(12):1300–9.

10. Tse JR, Engler AJ. Preparation of hydrogel substrates with tunable mechanical properties. Curr Protoc Cell Biol. 2010 Jun;Chapter 10:Unit 10.16.

11. Ran FA, Hsu PD, Wright J, Agarwala V, Scott DA, Zhang F. Genome engineering using the CRISPR-Cas9 system. Nat Protoc. 2013 Nov;8(11):2281–308.

12. Park J, Bae S, Kim J-S. Cas-Designer: a web-based tool for choice of CRISPR-Cas9 target sites. Bioinformatics. 2015 Dec 15;31(24):4014–6.

13. Rothbauer U, Zolghadr K, Muyldermans S, Schepers A, Cardoso MC, Leonhardt H. A versatile nanotrap for biochemical and functional studies with fluorescent fusion proteins. Mol Cell Proteomics. 2008 Feb;7(2):282–9.

14. Martinez-Arca S, Alberts P, Zahraoui A, Louvard D, Galli T. Role of tetanus neurotoxin insensitive vesicle-associated membrane protein (TI-VAMP) in vesicular transport mediating neurite outgrowth. J Cell Biol. 2000 May 15;149(4):889–900.